Transport and chemistry of formaldehyde by mesoscale convective systems in West Africa during AMMA 2006

Agnès Borbon,[1] M. Ruiz,[1] J. Bechara,[1] B. Aumont,[1] M. Chong,[2] H. Huntrieser,[3] C. Mari,[2] C. E. Reeves,[4] Georges Scialom,[5] T. Hamburger,[3,6] H. Stark,[7,8,9] C. Afif,[1,10] C. Jambert,[2] G. Mills,[4] H. Schlager,[3] and P. E. Perros[1]

Received 7 November 2011; revised 2 May 2012; accepted 3 May 2012; published 16 June 2012.

[1] In situ measurements of formaldehyde (CH_2O) onboard four European research aircraft in August 2006 as part of the African Monsoon Multidisciplinary Analysis (AMMA) experiment in West Africa are used (1) to examine the redistribution of CH_2O by mesoscale convective systems (MCS) in the tropical upper troposphere (UT), (2) to evaluate the scavenging efficiency (SE) of CH_2O by MCS and (3) to quantify the impact of CH_2O on UT photooxidant production downwind of MCS. The intercomparison of CH_2O measurements is first tested, providing a unique and consistent 3-D-spatially resolved CH_2O database in background and convective conditions. While carbon monoxide (CO) is vertically uplifted by deep convection up to 12 km, CH_2O is also affected by cloud processing as seen from its ratio relative to CO with altitude. A new observation-based model is established to quantify the SE of CH_2O. This model shows that convective entrainment of free tropospheric air cannot be neglected since it contributes to 40% of the convective UT air. For the 4 studied MCS, SE shows a large variability within a 4% to 39% range at a relative standard deviation of 30%, which is consistent with MCS features. A time-dependent photochemical box model is applied to convective UT air. After convection, 60% of CH_2O is due to its photochemical production rather than to its direct transport. Model results indicate that CH_2O directly injected by convection does not impact ozone and HOx production in the tropical UT of West Africa. NOx and anthropogenic hydrocarbon precursors dominate the secondary production of CH_2O, ozone and HOx.

Citation: Borbon, A., et al. (2012), Transport and chemistry of formaldehyde by mesoscale convective systems in West Africa during AMMA 2006, *J. Geophys. Res.*, *117*, D12301, doi:10.1029/2011JD017121.

1. Introduction

[2] Deep convection in the tropics plays a key role in determining the global atmospheric composition of the upper troposphere (UT) by the fast uplift of HOx radicals and ozone precursors from lower altitudes. However, the chemical consequences of deep convective systems are still uncertain. From an ensemble of 26 global atmospheric chemistry models, *Stevenson et al.* [2006] shows that the largest variability of the simulated ozone burden is in the tropics. The authors identify the representation of tropical deep convection as a major source of uncertainty in the models together with the isoprene emissions and chemistry, stratosphere-troposphere exchange and biomass burning emissions. *Martin et al.* [2002] also emphasizes the role of lightning NOx (nitrogen oxides) source associated with convection in the formation of the persistent southern tropical zonal wave-one pattern in total tropospheric ozone column. Overall, these studies suggest the complex coupling between dynamics and chemistry in convective processes

[1]Laboratoire Interuniversitaire des Systèmes Atmosphériques, IPSL, CNRS, UMR 7583, Universités Paris-Est Créteil et Paris-Diderot, Créteil, France.
[2]Laboratoire d'Aérologie, CNRS and Université de Toulouse, Toulouse, France.
[3]Institut für Physik der Atmosphäre, Deutsches Zentrum für Luft- und Raumfahrt, Oberpfaffenhofen, Germany.
[4]School of Environmental Sciences, University of East Anglia, Norwich, UK.
[5]Laboratoire Atmosphères Milieux Observations Spatiales, IPSL, Guyancourt, France.
[6]Now at Department of Applied Environmental Science, Stockholm University, Stockholm, Sweden.
[7]Earth System Research Laboratory, National Oceanic and Atmospheric Administration, Boulder, Colorado, USA.
[8]Now at Aerodyne Research, Inc., Billerica, Massachusetts, USA.
[9]Also at Cooperative Institute for Research in Environmental Sciences, University of Colorado Boulder, Boulder, Colorado, USA.
[10]Chemistry Department, Faculty of Sciences, Université Saint Joseph, Beirut, Lebanon.

Corresponding author: A. Borbon, Laboratoire Interuniversitaire des Systèmes Atmosphériques, IPSL, CNRS, UMR 7583, Universités Paris-Est Créteil et Paris-Diderot, 61 av. du Général de Gaulle, FR-94010 Créteil, France. (agnes.borbon@lisa.u-pec.fr)

and the limitations of its treatment in global chemistry models. More recently, *Tost et al.* [2010] pointed out the parameterization of deep convection as the main source of uncertainty in determining the sign and magnitude of ozone production in convective regions by global models. Indeed, not only moisture and energy are redistributed throughout the tropospheric column by deep convection but also chemical constituents of atmospheric interest. For instance, sensitivity studies to the convective transport of ozone and ozone precursors (Volatile Organic Compounds –VOC - and NOx) have shown the potential for both enhancement [*Lawrence et al.*, 2003] and reduction of ozone [*Doherty et al.*, 2005; *Lelieveld and Crutzen*, 1994] in the upper troposphere. The effect of deep convective transport on the redistribution of gaseous ozone precursors not only depends on dynamics but also on gas-phase and multiphase chemistry due to the presence of ice and water and cloud microphysics. In particular, chemistry and cloud microphysics affect the fate of soluble and chemically reactive ozone precursors such as formaldehyde (CH_2O). When simulating the redistribution of CH_2O within the anvil of a continental thunderstorm, results from various cloud-resolving models show dramatic differences in CH_2O mixing ratios up to a factor of 10 [*Barth et al.*, 2007b].

[3] Formaldehyde is a key intermediate produced during photochemical oxidation of VOC in the troposphere. It can also be emitted directly into the troposphere by biomass burning, incomplete combustion and by vegetation [*Carlier et al.*, 1986, and references therein]. Together with hydrogen peroxide (H_2O_2) and methyl hydroperoxide (CH_3OOH), photolysis of secondary CH_2O (e.g., from acetone photolysis) is an important source of HOx in the UT [*Jaeglé et al.*, 1997; *McKeen et al.*, 1997; *Cohan et al.*, 1999; *Folkins and Chatfield*, 2000]. In the convectively influenced air in the UT, excess formaldehyde (i.e., higher than background concentrations) can be either directly transported from lower altitudes or be produced via the injection of precursors such as non-methane hydrocarbons (NMHC) [*Fried et al.*, 2008b]. Global modeling studies indicate that the impact of convected CH_2O on UT HOx is spatially variable. While the convective injection of peroxides is the dominant source of HOx over tropical oceans [*Prather and Jacob*, 1997; *Jaeglé et al.*, 1997], convected aldehydes dominate over the continent [*Müller and Brasseur*, 1999]. However, these theoretical calculations suffer from a lack of observations, and uncertainties regarding convection characteristics. As ozone production in the UT is almost directly proportional to the HOx mixing ratios [*Jaeglé et al.*, 1998; *Müller and Brasseur*, 1999], a comprehensive knowledge of upper tropospheric CH_2O sources is thus essential for understanding UT ozone in the tropics. Measurements of CH_2O in the UT impacted by convection, together with H_2O and CH_3OOH, have been acquired and examined over the last decade in different regions of the world: tropical Pacific during PEM-Tropics B [*Raper et al.*, 2001; *Ravetta et al.*, 2001; *Mari et al.*, 2002], Mediterranean basin during MINOS [*Lelieveld et al.*, 2002; *Kormann et al.*, 2003], central Europe during UTOPIHAN [*Colomb et al.*, 2006; *Stickler et al.*, 2006] and North America and North Atlantic during INTEX-NA [*Fried et al.*, 2008a]. There is however a paucity of similar measurements and analyses over tropical continental regions associated with deep convective events.

[4] Continental West Africa encompasses a large domain and has south-north landscape gradient with sharp transitions from ocean to forest and from forest to desert at around 6° N and 12° N, respectively [*Janicot et al.*, 2008]. The West African Monsoon (WAM) is characterized by convective activity as a result of the abrupt change in atmospheric circulation relative to the ITCZ (Intertropical Convergence Zone) position between June and July. Deep convection during the WAM season occurs in relatively large organized westward propagating systems known as mesoscale convective system (MCS) [*Lafore et al.*, 2011]. MCSs over West Africa have a well-defined structure that can be maintained while they propagate. A common feature is the well-marked stratiform structure of the precipitating trailing anvil cloud, which contrasts with the convective structure of the leading edge [*Houze*, 1989; *Chong*, 2011]. Over West Africa, ozone precursors are mainly emitted from soils and vegetation [*Guenther et al.*, 1995; *Serça et al.*, 1998] and urban areas [*Minga et al.*, 2010]. When these emissions are co-located with MCSs, emitted gases (carbon monoxide – CO -, NMHC) and aerosols can be transported quickly and efficiently to the upper troposphere by convective updraft. This transport modifies the UT mixing ratios of ozone and other trace gases [*Ancellet et al.*, 2009; *Saunois et al.*, 2009; *Law et al.*, 2010; *Bechara et al.*, 2010; *Huntrieser et al.*, 2011], water vapor availability [*Homan et al.*, 2010] and aerosol concentrations [*Borrmann et al.*, 2010].

[5] The goal of this study is to examine the redistribution of formaldehyde by MCS developing over West Africa, to quantify their transport efficiency on formaldehyde into the tropical UT and to determine the relative importance of UT formaldehyde sources on photooxidant production downwind of MCS. This work combines observations and 0-D photochemical box modeling. Observations were collected over West Africa during the monsoon period (July–August 2006) as part of the African Monsoon Multidisciplinary Analysis (AMMA) experiment. Airborne observations of formaldehyde were collected at various altitudes from 0 to 12 km and under various conditions (background and convective).

2. Methodology

2.1. Overview of the AMMA SOP2-a2 Airborne Campaign

[6] AMMA is an international program designed to improve the understanding of the monsoon variability and its consequences on the environment and population in West Africa at daily to-interannual timescales [*Redelsperger et al.*, 2006]. AMMA was divided into several special observation periods (SOPs) including the Peak-Monsoon SOP (#2-a2) associated with convective activity. Four aircraft platforms were deployed during SOP2-a2 from July 25th to August 31st 2006. Two French aircraft, the ATR-42 and the French F-Falcon-20 operated by SAFIRE, as well as the UK BAe-146 operated by FAAM, were based in Niamey (Niger). The German D-Falcon-20 operated by DLR was based in Ouagadougou (Burkina Faso). Given the complementary performances of the aircraft (altitude and radius range), their deployment aimed to obtain a full description of the composition of the West African troposphere under undisturbed and convective conditions. The four aircraft equipped with

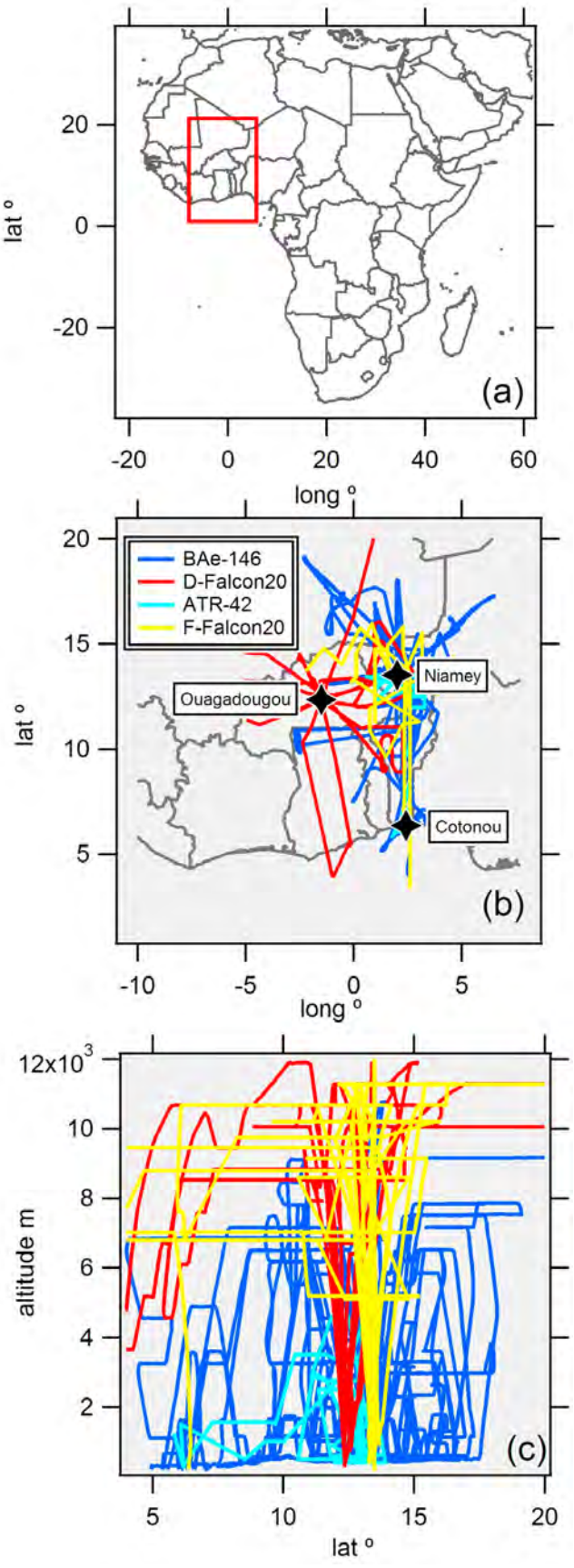

formaldehyde instruments on-board were deployed throughout a large 3-D-domain (long.: −8°E-5°W, lat. 4°N–20°N, alt.: 0–12 km) (Figure 1).

[7] The airborne strategy consisted of sampling the MCS inflow and outflow by exploring the boundary layer composition (ATR-42 and BAe-146) and performing anvil transects at various distances from the MCS core (French and German Falcon-20). A total of 55 flights (more than 150 h) of, at least, three hours each were performed. At the same time, an important monitoring network at the surface complemented the aircraft instrumental setup. In particular, this network included high-time-resolution surface rainfall gauges and two C-band Doppler radars. These sensors will be further discussed in section 5.5. as these data will support the interpretation of the estimated scavenging efficiency of CH_2O.

2.2. Airborne Instrumentation

[8] The core instrumentation on-board the 4 aircraft, including formaldehyde and inorganic trace gases measurements (CO and ozone), is described in detail in the supplementary material of *Reeves et al.* [2010]. Only the principles and performances of airborne formaldehyde measurements are reported here.

2.2.1. AMOVOC Technique on the ATR-42 and F-Falcon20

[9] AMOVOC (Airborne Measurements of Volatile Organic Compounds) operated by the LISA group, is an offline automatic sampler designed to collect a wide range of VOC on various trapping devices at constant temperature: solid sorbent tubes and a liquid glass coil scrubber. Sampling and analysis by AMOVOC and its aircraft integration have been already described by *Bechara et al.* [2008]. During AMMA, two AMOVOC were simultaneously deployed on both French aircraft for C4-C9 NMHC and CH_2O sampling at 10-min-time intervals and 20°C-regulated temperature. The detection limits (DL) for NMHC were less than 10 ppt and the precision was lower than 24%. In parallel, CH_2O was first collected in a liquid coil scrubber at an airflow of 2L.min^{-1} in an aqueous 2,4-dinitrophenylhydrazine (DNPH) acidified solution. Liquid samples were collected in 3 mL-vials. Analysis was performed at the laboratory by High Performance Liquid Chromatography-UV visible at 380 nm (Waters). The scavenging efficiency of formaldehyde at 20°C was estimated to be 84%. The method was successfully adapted from *Lee et al.* [1996] with the same performances. Although O_3 could affect these results due to the absence of an O_3 scrubber in the inlet, *Gilpin et al.* [1997] and *Fried et al.* [2002] showed excellent agreement of this approach with tunable diode laser absorption spectroscopic (TDLAS) measurements in the presence of ambient O_3 levels.

2.2.2. Hantzsch Reaction Technique on the BAe-146 and D-Falcon20

[10] Both of the CH_2O instruments operated by the UEA and DLR groups on board the BAe-146 and D-Falcon-20,

Figure 1. (a) West Africa domain explored during AMMA and (b and c) 2-D-flight tracks during AMMA SOP2-a2. The three major urban areas on the domain are indicated by the black crosses.

respectively, employed the fluorimetric Hantzsch reaction in the liquid phase. The CH_2O instruments were described previously by *Still et al.* [2006], *Cárdenas et al.* [2000] and *Junkermann and Burger* [2006]. On the BAe-146, the instrument had a DL of 54 pptv for 3 min-averaged data. On the D-Falcon-20, the instrument (Aerolaser AL4021) had a precision and accuracy of 10% and 20%, respectively, for 60 s-averaged data. The DL was 50 pptv [*Reeves et al.*, 2010]. *Gilpin et al.* [1997] showed excellent agreement in ambient CH_2O measurements acquired in Boulder, Colorado, with this technique compared to TDLAS when the Hantzsch measurements were normalized to the TDLAS standards.

2.3. Chemical Box Model

[11] The evolution of the chemical composition of the convective outflow plume in the UT is simulated by a 0-D photochemical box model that incorporates the Master Chemical Mechanism - version 3 (MCM v3.1) [*Saunders et al.*, 2003; *Jenkin et al.*, 2003]. The model developed here consists of a box representing the convective outflow plume. The model calculates the production and loss over time of O_3, CO, NOx (NO and NO_2), NOy, HOx and VOCs (including formaldehyde). The dilution of the plume is treated as a first order process of constant rate. The expansion of the convective box leads to the injection of species from the background UT into the convective box. The estimation of the dilution rate is constrained from the airborne observations of an inert tracer (here, CO) and is discussed in section 6.1.1.

[12] In this study, an average convective case is considered. The duration of the simulation is set to 3 days. The model is initialized with mean airborne observations and physico-chemical conditions of the West Africa UT during the AMMA SOP2-a2 at 13°N and at 12 km altitude, which is the mean altitude of MCS outflow flights. Meteorological parameters are the averages of those observed by the UT Falcon-20 flights during SOP2-a2. Temperature and relative humidity are fixed to 223 K and 70%, respectively. Photolysis constants are calculated with an external module (Tropospheric Visible Ultraviolet model) [*Madronich and Flocke*, 1998]. The different scenarios and the initial conditions of the composition of the convective and background UT will be discussed in more details in section 6.

3. Construction of the CH_2O Database

[13] Measurements of CH_2O at low ppb levels remain challenging. While past intercomparisons at ground level revealed fair consistency between state-of-the-art instruments (incl. Hantzsch fluorimetric technique) [*Hak et al.*, 2005, and references therein], the presence of humidity and ozone may cause important biases [*Wisthaler et al.*, 2008]. Thus, a thorough verification of CH_2O measurements is systematically needed to support data interpretation, especially with regard to airborne measurements for which the quantitative transfer of CH_2O through the inlet is another critical issue [*Wert et al.*, 2003]. During the AMMA SOP2-a2, CH_2O measurements were performed onboard 4 different platforms, using two different techniques and operated by three different groups. It was therefore crucial to compare the different CH_2O data sets from the different instruments to ensure their consistency. Intercomparison flights took place on August 16th 2006 as described in Appendix A of the overview by *Reeves et al.* [2010]. However, testing the consistency of the CH_2O data set was limited to the BAe-146 and D-Falcon20 at only two flight levels: FL100 (697 hPa) and FL190 (485 hPa). Therefore, it was decided, in this study, to extend the intercomparison to the scientific flights.

[14] The challenge here was to identify photochemically equivalent situations for which the CH_2O data set could be compared given the lack of temporally coincident CH_2O measurements and the spatial and temporal variability of CH_2O concentrations. During AMMA, the distribution of CH_2O concentrations could be influenced by: the north-south gradient of surface emissions of CH_2O and its VOC precursors [*Bechara et al.*, 2010; *Murphy et al.*, 2010], the long range transport of air masses influenced by biomass burning from the Southern Hemisphere [*Mari et al.*, 2008], the vertical distance from primary sources, and the environmental conditions (sunlight radiation, temperature and relative humidity) affecting its lifetime and gas-liquid partitioning. First, CH_2O data were divided into 1°-latitude × 500 m-altitude bins. Three zones, related to aircraft pairs, were identified but only one zone (12–13°N latitude by 0–6.5 km altitude) is reported here as no photochemically equivalent situations were found for the two other zones. Then, in each zone, the statistical equivalence of the means of some physico-chemical tracers was tested by a multistep hypothesis test procedure [*Shapiro and Wilk*, 1965]. The goal is to isolate photochemically equivalent bins suitable to test the equivalence of CH_2O observation means. This procedure includes normality test, variance test (Snedecor) and mean test (Student or Welch). If the means of CH_2O data are found to be equivalent in all photochemically equivalent bins, then all the CH_2O data from both aircraft are comparable: they can be combined into a single data set. Measurements of the physico-chemical tracers have to be redundant and comparable on the four platforms. These tracers are: CO, a primary combustion product which is a tracer of anthropogenic and biomass burning emissions, ozone, a secondary product which is a tracer of photochemical processing and relative humidity (RH) as an indicator of cloud presence. Together, these tracers reflect the history of air masses: emissions, photochemical processing and convective cloud influence. Radiation and temperature conditions, typical of the wet monsoon period, did not change from one day to another. Only data collected between 8:00 and 18:00 LT were considered in the test. The number of data points per bin had to be higher than 9 to proceed to the multistep hypothesis test procedure (criteria for Welch test application).

[15] Results are provided in Figure 2 for zone 1. The vertical profiles of CO and ozone follow an opposite trend as already described by *Reeves et al.* [2010] and *Bechara et al.* [2010]. While the vertical profiles of CO and ozone overlap quite well for the BAe-146 and D-Falcon20, the multistep hypothesis test procedure was applied to test the normality and equivalence of the pairs of data for each altitude bin. CO and ozone are found to be equivalent for only 4 altitude bins in zone 1. Formaldehyde mixing ratios were then statistically compared for each of the four bins by applying the multistep hypothesis test procedure: they were found to be equivalent.

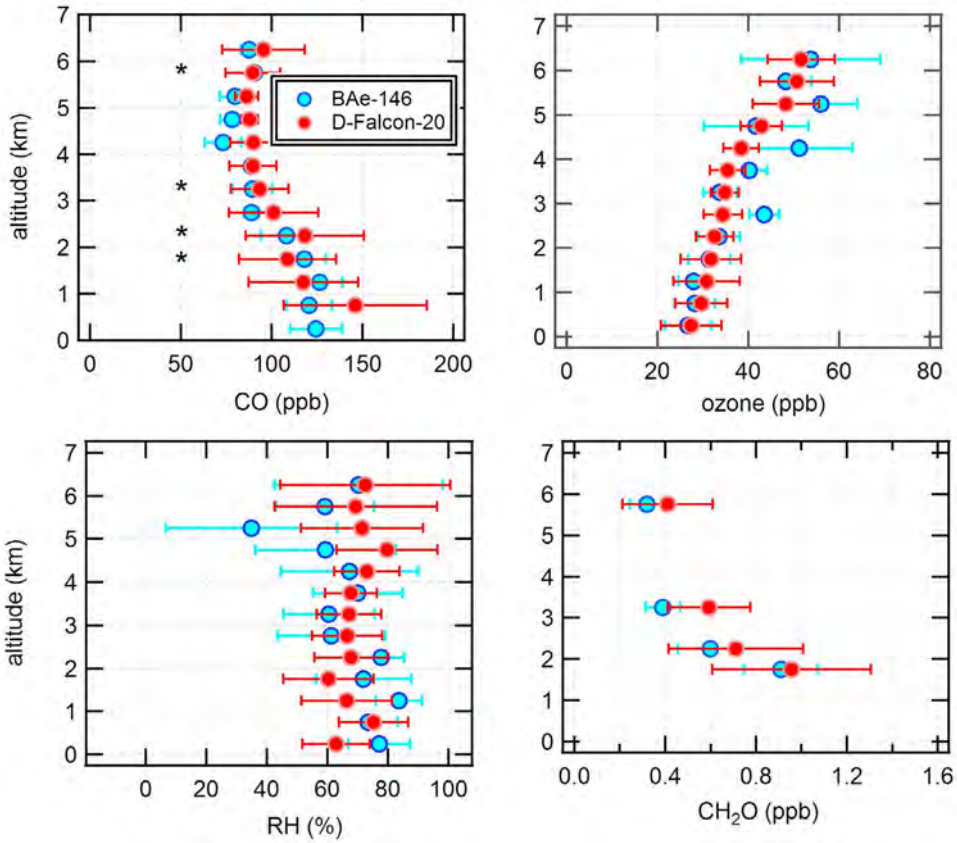

Figure 2. Comparison of the 3 physico-chemical tracers (CO, ozone and relative humidity, RH) and CH_2O from the BAe-146 and D-Falcon20 aircraft in zone 1. The stars mark the altitude bins where physico-chemical tracers are statistically comparable.

[16] Finally, only formaldehyde data collected on-board the BAe-146 and D-Falcon20 can be combined into a single and unified data set for further analysis. The multistep hypothesis step procedure has shown their statistical equivalence while no conclusion could be made on the statistical equivalence of formaldehyde for the French platforms (ATR42 and F-Falcon20).

4. Vertical Profile of CH_2O Over West Africa During the WAM Season

[17] The vertical distribution of formaldehyde mixing ratios is shown in Figure 3a and compared with the one of CO. In the boundary layer, both compounds show great variability as they are influenced by the north-south gradient of surface emissions over a 10° latitude range [*Murphy et al.*, 2010; *Reeves et al.*, 2010]. Below 8 km, CO and formaldehyde mixing ratios both decrease with altitude. Above 8 km, CO shows the "C-shaped" profile signature of deep convective transport [*Blake et al.*, 1996; *Bechara et al.*, 2010; *Reeves et al.*, 2010] which uplifts gaseous trace gases from the lower troposphere to the upper troposphere (12 km). Unlike CO, formaldehyde does not show this "C-shaped" profile: its altitude profile is fairly constant from 8 to 12 km.

[18] In order to get a more quantitative sense of the fate of formaldehyde with altitude, a ratio r (r = Δ[CH_2O]z/Δ[CO] z) is determined. r is given by the slope of a linear regression fit on [CH2O]z versus [CO]z data (Figure 3b). The data are color-coded with the altitude. Two populations can be distinguished depending on the altitude range. From the surface to 8 km, the ratio is 24 ppt [CH_2O]/ppb [CO] and [CH_2O] and [CO] both decrease with altitude. Conversely, above 8 km, the ratio is 3 ppt [CH_2O]/ppb [CO] and [CH_2O] and [CO] both increase with altitude. This lower value at higher altitudes is the result of an enrichment of the upper troposphere in favor of CO rather than formaldehyde due to convective transport. In particular, this reflects the additional effect of cloud processing during the convective transport of CH_2O compared with CO. Its relative importance will be discussed in detail in the following section.

5. Transport Efficiency of Formaldehyde

[19] The objective here is to evaluate the relative importance of the processes affecting formaldehyde concentrations during its transport to the UT and especially its loss by wet scavenging.

5.1. Methods

[20] The method commonly used to estimate the scavenging efficiency is based on observations and was first proposed by *Cohan et al.* [1999]. This two-component-mixture model considers the mixing ratio of a non-soluble species X in the convective UT as a function of its boundary layer mixing ratio and UT background mixing ratio. This approach was supported by *Bechara et al.* [2010] who

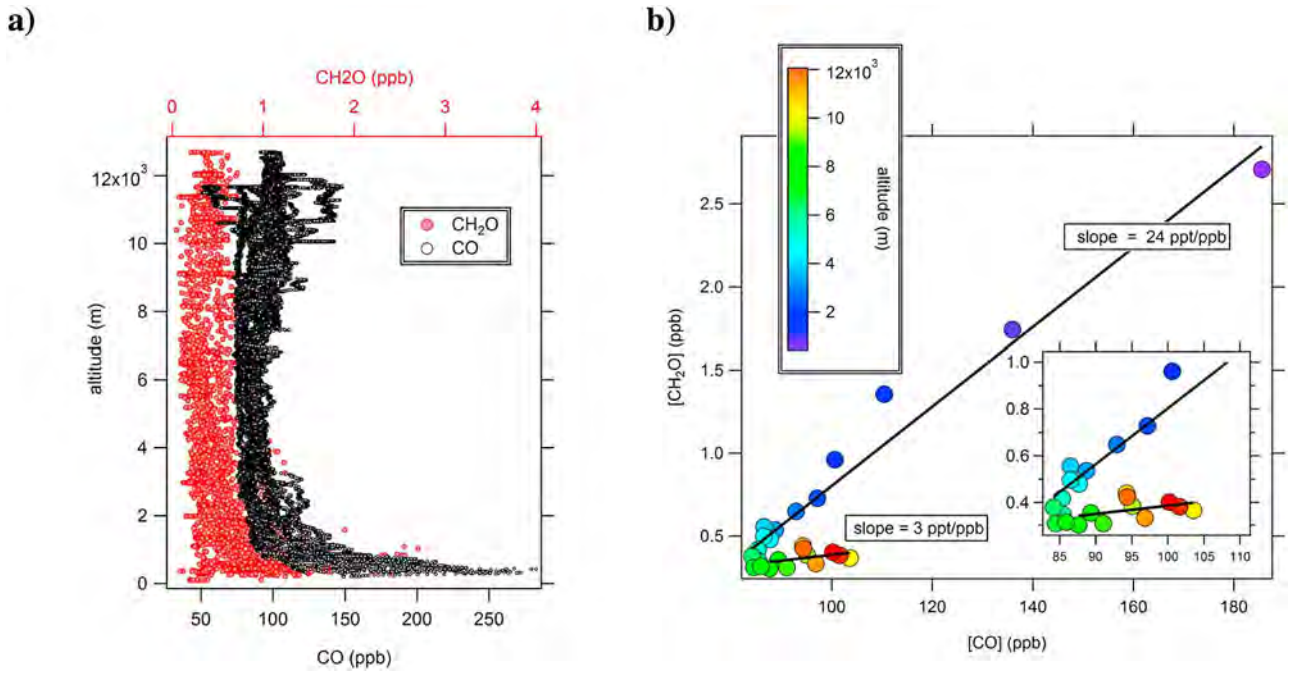

Figure 3. (a) Vertical profiles of CH_2O and CO mixing ratios from airborne measurements and (b) scatterplots of CH_2O versus CO average mixing ratios per 500-m altitude bin, color-coded by altitude. The dark line is the linear regression fit below and above 6 km.

showed that the observed chemical composition of MCS outflow over West Africa was dependent on surface emission composition. This model gives:

$$X_{CONV} = \beta X_{BL} + (1-\beta)X_{UT} \quad (1)$$

where X_{CONV} (respectively X_{BL} and X_{UT}) is the mixing ratio of the non-soluble species in the convective outflow (respectively in the boundary layer and in the upper troposphere). β represents the fraction of the boundary layer air present in fresh convective UT air. For a soluble species Y, equation (1) becomes:

$$Y_{CONV} = (1-SE)\beta Y_{BL} + (1-\beta)Y_{UT} \quad (2)$$

where Y_{CONV} (respectively Y_{BL} and Y_{UT}) is the mixing ratio of the soluble species in the convective outflow (respectively in the boundary layer and in the upper troposphere). SE stands for the scavenging efficiency and is species-dependent. From (2), SE can be written as:

$$SE = 1 - \frac{Y_{CONV} - (1-\beta)Y_{UT}}{\beta Y_{BL}}. \quad (3)$$

[21] While this model has been used in recent studies [*Stickler et al.*, 2006; *Bertram et al.*, 2007; *Bechara et al.*, 2010], other studies suggest that entrainment and detrainment from intermediate layers and beyond cannot be neglected [*Prather and Jacob*, 1997; *Mari et al.*, 2000; *Lopez et al.*, 2006; *Barthe et al.*, 2011]. To account for and test the contribution of entrainment and detrainment processes, a new three-component mixture model was defined, which considers the new potential reservoir of species at intermediate levels in the troposphere. Given β, the fraction of boundary layer air, and α, the fraction of mid-level free tropospheric air entrained in the cloud, the equation of the non-soluble species X transported by deep convection is:

$$X_{CONV} = \beta X_{BL} + \alpha X_{FT} + (1-\beta-\alpha)X_{UT} \quad (4)$$

with $\beta + \alpha \leq 1$.

[22] Similarly to the two-component mixture model, the scavenging efficiency of a soluble species Y can be derived from:

$$SE = 1 - \frac{Y_{CONV} - (1-\beta-\alpha)Y_{UT}}{\beta Y_{BL} + \alpha Y_{FT}}. \quad (5)$$

[23] To determine SE, one has first to evaluate the α and β fractions.

5.2. Hypothesis and Uncertainties

[24] Equations (3) and (5) imply that the scavenging efficiency is only driven by dynamics (entrainment and detrainment), microphysical processes (condensate profile) and the ability of formaldehyde to be incorporated into cloud droplets. The latter includes the mass transfer from the gas to the aqueous phase and aqueous chemical reactions. After dissolution, formaldehyde almost immediately hydrates to form a gem diol ($CH_2(OH)_2$), which rapidly reacts with the OH radical [*Lelieveld and Crutzen*, 1991]. In other words, both models rely on the assumption that gas-phase chemistry, particularly secondary photochemical production, during vertical transport can be neglected. Here, we propose to discuss this assumption regarding its three major photochemical depletion and formation processes: photodissociation, oxidation by the OH radical and secondary production by its NMHC precursors. In particular, the lifetime of formaldehyde is estimated and compared with the convective transport

timescale of 25 ± 10 min determined by *Bechara et al.* [2010] for MCS over West Africa.

[25] *CH_2O photodissociation.* photolysis frequency depends on the actinic flux that increases with altitude and is affected in different ways within and below the cloud due to the combined effect of backscattering and diffusion [*Lelieveld and Crutzen*, 1991]. Here, we estimate the photolysis frequency of formaldehyde, j(CH_2O). Only the photolysis frequency of NO_2, j(NO_2), was available on-board the BAe-146 [*Monks et al.*, 2004]. Following *Kraus and Hofzumahaus* [1998], the photolysis frequency of formaldehyde is estimated from its linear relationship with j(NO_2) derived from actinic flux data measured from an airborne spectroradiometer, AFSR, under various atmospheric conditions [*Stark et al.*, 2007]. From this linear fit, j(NO_2) from the BAe-146 is converted into j(CH_2O). The BAe-146 flight of August 17th 2006 provides a representative picture of the variability and magnitude of j(NO_2) at altitudes up to 8 km, inside and outside the cloud. Within the cloud, j(NO_2) decreases to 4×10^{-3} s^{-1}, an order of magnitude lower than its average value in clear sky conditions ($1.5–2.0 \times 10^{-2}$ s^{-1}). Therefore, j(CH_2O) within the cloud can be estimated to roughly equal 3.6×10^{-5} s^{-1}, which corresponds to a photolysis lifetime ($\tau_{photolysis}$) of 7.8 h. Given the definition of lifetime, no more than 2% of CH_2O is photolyzed during its vertical transport. As a consequence, the assumption of no CH_2O photodissociation during its convective transport from the boundary layer to the UT sounds reasonable.

[26] *Gas-phase oxidation of CH_2O by OH.* OH mixing ratios are highly variable in time and space during the WAM season as seen from its measurements on-board the BAe-146 [*Commane et al.*, 2010]. However, its median mixing ratio is relatively constant with altitude: 0.2 ppt (5×10^6 molecules.cm^{-3}) in clear sky conditions. The highest mixing ratio observed between the top of the boundary layer and 12 km is 0.6 ppt (1.5×10^7 molecules.cm^{-3}). Given the rate constant of 8.5×10^{-12} cm^3.$molecule^{-1}$.s^{-1} in the 220 K–298 K range [*Sander et al.*, 2011] and an OH mixing ratio of 1.5×10^7 molecules.cm^{-3}, the lifetime of formaldehyde due to OH oxidation (τ_{OH}) is 2 h. Considering the efficient uptake of OH onto cloud droplets, τ_{OH} should be seen as a lower limit within and below the cloud. Indeed, cloud chemistry models [*Lelieveld and Crutzen*, 1994] and field observations [*Mauldin et al.*, 1997] found that gas-phase OH concentrations in cloud can be depleted by a factor 2 to 3 relative to clear-sky conditions. Therefore, the estimated τ_{OH} is expected to be 2 to 3 times higher (4 to 6 h). Given the definition of lifetime, no more than 4% of CH_2O is oxidized by OH during its vertical transport. As a consequence, the gas-phase oxidation of formaldehyde by OH can be neglected during convective transport.

[27] *Secondary production of CH_2O by NMHC precursors. Bechara et al.* [2010] showed the efficiency of MCS in the vertical transport of NMHC precursors to the UT. Here, the oxidation of isoprene, the main precursor of secondary formaldehyde, is considered during convective transport. To estimate the concentration of formaldehyde attributable to isoprene photooxidation ($CH_2O_{isoprene}$) the method described by *Duane et al.* [2002] is applied:

$$CH_2O_{isoprene} = 0.61 \times \Delta isoprene \quad (6)$$

where 0.61 is the mean fractional yield of CH_2O from the first oxidation stage of isoprene reported by *Sprengnether et al.* [2002, and reference therein] and Δisoprene is the concentration of isoprene that is lost through reaction during its transport. This calculation assumes that all the CH_2O formed from isoprene oxidation reaches the UT.

$$\Delta isoprene = (\beta \times isoprene_{BL} + \alpha \times isoprene_{FT}) - isoprene_{conv} \quad (7)$$

where β and α are the respective fraction of isoprene transported from the boundary layer and free troposphere as described in section 5.1., $isoprene_{BL(FT)}$ is the initial concentration of isoprene in the boundary layer (free troposphere) and $isoprene_{conv}$ is the final concentration of isoprene after convective transport.

[28] $Isoprene_{BL(FT)}$ is derived from *Murphy et al.* [2010] for the Niamey region (0.067 ppb) and the tropical mosaïc forest region (0.604 ppb). $Isoprene_{conv}$ can be deduced from the following photochemical equation:

$$isoprene_{conv} = \exp^{(-k_{OH} \times [OH] \times t)} \times (\beta \times \text{isoprene BL} + \alpha \times \text{isoprene FT}) \quad (8)$$

where k_{OH} of isoprene equals 100×10^{-12} cm^3.$molecule^{-1}$.s^{-1} at 298 K [*Atkinson*, 2000], t is the duration of convective transport (25 min).

[29] By combining equations (7) and (8), Δisoprene can be expressed as:

$$\Delta isoprene = (\beta \times isoprene_{BL} + \alpha \times isoprene_{FT}) \cdot \left(1 - \exp^{(-k_{OH} \times [OH] \times t)}\right). \quad (9)$$

[30] By combining equations (6) and (9), $CH_2O_{isoprene}$ is estimated to be 13% and 33% of CH_2O transported by convection for the Niamey region and for the tropical forest region, respectively. For a transport time scale of 25 min, the secondary production of formaldehyde by isoprene cannot be neglected. Both values of $CH_2O_{isoprene}$ provide upper limits to the secondary production of formaldehyde as the OH mixing ratio was taken in clear sky conditions.

[31] Finally, the photochemical production of CH_2O during convective transport over regions influenced by biogenic emissions can be significant while its photochemical depletion is small (<6%). This secondary production term is the main source of uncertainty in the estimation of SE as it affects the Y_{CONV} term in equations (3) and (5). The uncertainty on SE calculation is therefore set to ±30%.

5.3. Calculation of the β and α Fractions

[32] Equation (4) can be constrained, at least, with the observed mixing ratios of CO and VOCs. Ideally, a case-by-case calculation should be carried out to take into account the variability of entrainment and detrainment processes. However, the vertical profiles of VOCs throughout the 12-km column are only available on-board the two French aircraft, the ATR-42 and the F-Falcon-20 [*Bechara et al.*, 2010], which did not fly at the same time. Consequently, average observations from the MCS flights performed by the French aircraft are considered, including the one on August

Table 1. Input Data and Results for the β, α and δ Calculation[a]

	X_{BL} (<2 km) in ppb	X_{FT} (2–8 km) in ppb	X_{UT} (10–12 km) in ppb	X_{CONV} (10–12 km) in ppb	β	α	δ
Airborne Observations (This Study)							
Benzene	0.11	0.08	0.02	0.08	**0.50**	**0.41**	**0.88**
Toluene	0.60	0.12	0.17	0.37			
CO	131	94	89	105			
3D-CRM Model From Barthe et al. [2011]							
TR1	1	0	0	0.35	**0.35**	**0.45**	
TR2,TR3,TR4	0	1	0	0.45			

[a]See text for details. The boldfacing corresponds to the results whereas other numbers are the inputs used for calculation.

15th 2006 retained as a case study in section 5.4. Here a third variable is introduced, δ, which corresponds to the detrainment term in equation (4) with $\delta = \beta + \alpha$. The equation to be solved becomes:

$$X_{CONV} = \beta X_{BL} + \alpha X_{FT} + (1 - \delta) X_{UT}. \quad (10)$$

[33] Airborne observations of CO, benzene and toluene are used (Table 1) to quantify α, β and δ. These results are compared with model outputs from *Barthe et al.* [2011], who used the 3-D cloud resolving model MesoNH to simulate the redistribution of 5 passive tracers for an MCS passing over West Africa on August 14th–15th 2004. The five tracers were initially confined within 5 horizontal homogeneous layers. From Figure 9 in *Barthe et al.* [2011], one can deduce the relative contribution of the boundary layer tracer between 0 and 2 km (named TR1 in the cited paper) and the free troposphere tracers (sum of the named TR2, TR3 and TR4 in the cited paper) to the mixing ratio in the upper troposphere. In the model, the initial background values of the idealized tracers were set to zero. Therefore, equation (10) can be simplified to:

$$X_{CONV}^{MODEL} = \beta^{MODEL} X_{BL}^{MODEL} + \alpha^{MODEL} X_{FT}^{MODEL}. \quad (11)$$

[34] Input data and results of the β, α and δ calculation are reported in Table 1. Airborne observations yield $\beta = 0.50$ and $\alpha = 0.41$ while the model predicts a total contribution of free tropospheric tracers α^{MODEL} of 0.45 and a contribution of the boundary layer tracer β^{MODEL} of 0.35. Moreover, the detrainment term δ differs from the sum $\beta + \alpha$ by only 3%, indicating the mutual consistency of the estimated parameters. Finally, both model and observations show that the fraction of free tropospheric mid-level air present in the fresh convective outflow is close to 40–50% and cannot be neglected in the calculation of scavenging efficiency.

5.4. Case Studies

[35] To evaluate the SE of CH_2O, one has to establish a set of representative conditions to determine the four terms: Y_{CONV}, Y_{FT}, Y_{UT} and Y_{BL} in equation (5) where Y is the mixing ratio of formaldehyde.

[36] *Y_{CONV} and Y_{UT}.* To minimize the secondary production of CH_2O downwind of MCS, we only consider the flight tracks of the D-Falcon20 above 10 km altitude and at the edge of the MCS to determine Y_{CONV}. This is done by superimposing flight tracks on Meteosat-IR images. This analysis combines time series of several trace gases, including CH_2O as well as NO (nitrogen monoxide) and CO. The concomitant increase of NO and CO mixing ratios in the UT indicates the influence of fresh convection. From this analysis, four flights are retained for determining Y_{CONV}: August 6th (decaying MCS over Burkina Faso), August 7th (large MCS over Mali), and two flights on August 15th (decaying MCS west of Niamey and an MCS over Benin). Flight tracks, satellite images and two time series data are reported in Figure 4. As an example, for the flight on August 7th, the X_{CONV} term is determined for the time period 1:40–2:15 UTC when NO and CO mixing ratios both show a sharp increase.

[37] The examination of Meteosat-IR images and time series of trace gases shows that the UT sampled by the D-Falcon20 is influenced by convection most of the time, except on August 13th (decaying small thunderstorm over Burkina and further south) (Figure 4). During this flight, the time series of NO and CO mixing ratios suggest the influence of convection on UT air excepted during the period around 11:30 UTC when the distance to the convective region and the low mixing ratios of trace gases point to background conditions. This period of background conditions is used to determine Y_{UT}. The derived mixing ratio of 0.17 ± 0.08 ppb for formaldehyde is in agreement with previous values reported for the non-influenced free and upper troposphere by convection (0.165 ppbv by *Fried et al.* [2008b]).

[38] *Y_{FT}.* We combine and average formaldehyde observations from the D-Falcon20 for each of the four flights and BAe-146 for the same latitude-longitude area between 2 and 8 km as there were no-time coincident flights for the two aircraft.

[39] *Y_{BL}.* Since Y_{BL} represents the mixing ratios of the MCS inflow, we determine Y_{BL} by averaging formaldehyde observations from the BAe-146 flights in the troposphere below 2 km altitude, at the same time of the day and in the area of the MCS passage.

5.5. Scavenging Efficiency of CH_2O: Results and Discussion

[40] The results of the scavenging efficiency (SE) calculations from equations (3) and (5) are reported in Table 2 for the four MCS case studies. The Coefficient Enhancement Factors (CEF) of formaldehyde are also reported: they represent the ratio of the formaldehyde mixing ratio in the convective UT to the one in the background UT [*Mari et al.*, 2000]. While part of formaldehyde is scavenged during convective transport, all CEF values, which are greater than 1.5, highlight the enrichment of background UT air in formaldehyde by deep convection as also seen from Figure 3. In half of the cases, the commonly used two-component mixture model gives negative scavenging efficiencies. This implies that the term (Y_{CONV}-Y_{UT}) in equation (3) is greater than β(Y_{BL}-Y_{UT}) while it should be, at least, equivalent. Therefore, a source term is missing in the expression of SE that is attributed here to additional entrainment of free troposphere air rather than a formaldehyde secondary production as discussed in section 5.2. The two-component mixture model seems to underestimate CH_2O scavenging efficiency compared with the new three-component mixture model which, therefore, appears more appropriate. As a consequence, for the following discussion,

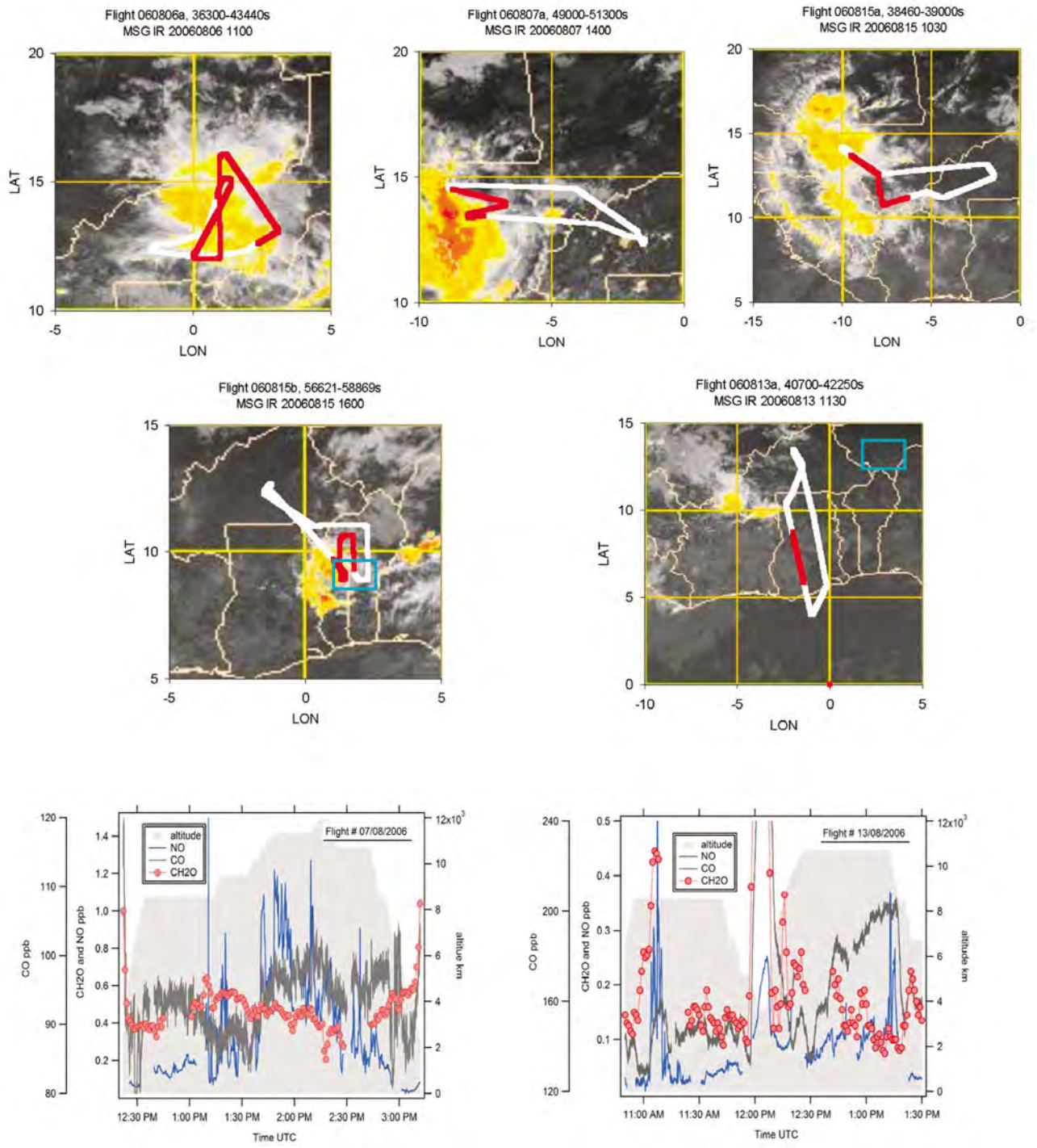

Figure 4. Flight tracks of the D-Falcon20 superimposed on MSG-IR satellite images and time series of trace gases (incl. CH_2O) for two of these flights (#13/08/2006 and #07/08/2006). Legs color-coded in red are the segments of the flight tracks selected for the calculation of the scavenging efficiency of CH_2O (see text in section 5.4). The blue squares on MSG-IR images correspond to the location of the AMMA-CATCH mesoscale sites (see text in section 5.5).

only the SE calculated using the new three-component mixture model is considered. The scavenging efficiency of CH_2O is highly variable within an order of magnitude among the 4 MCS and a relative uncertainty of 30% (see section 5.2). The SE variability is comparable with the most recent cloud resolving model study by *Barth et al.* [2007a, 2007b].

[41] The SE of formaldehyde depends on chemistry (gaseous and aqueous), dynamics (updraft velocities, turbulent entrainment) and cloud microphysics (ice to water ratios,

Table 2. Coefficient Enhancement Factor (CEF) and Scavenging Efficiency SE (± Absolute Error) of Formaldehyde Derived From Observations by Applying the Two-Component Model (2-var Model) and the 3-Component Model (3-var Model)[a]

Flight	Flight			
	# 06082006	# 07082006 Niamey Flight	#15082006a	# 15082006b Oueme Flight
Domain	Lat: 11°–16° N Long:0.0°–2.5° E West Niamey	Lat: 12°–15° N Long:-9°-1° W SWest Niger	Lat: 10°-15° N Long:-9°-1° W Mali- West Niamey	Lat: 9°-13° N Long:-2° W-2.5° E North Benin
$Y_{BL < 2\ km}$ ppb	0.83	0.84	0.84	0.83
$Y_{FT\ (2–8\ km)}$ ppb	0.39	0.37	0.37	0.57
Y_{CONV} ppb	0.45	0.51	0.38	0.66
Y_{UT} ppb	0.17	0.17	0.17	0.17
CEF	**1.81**	**1.53**	**2.04**	**2.62**
SE –2 var. model	**9%**	**26%**	**<0**	**<0**
SE – 3 var. model	***26 ± 8%***	***39 ± 12%***	***13 ± 4%***	***4 ± 1%***

[a]Y is formaldehyde mixing ratios used for calculation. The italics highlight the results of the new model developed in this work and on which the discussion is based on. The boldfacing corresponds to the results whereas other numbers are the inputs used for calculation.

condensate profiles, degassing during droplet freezing) [*Mari et al.*, 2000; *Leriche et al.*, 2000; *Barth et al.*, 2007a]. The estimated SE values are now discussed with regard to the observed MCS features to provide, at least, a qualitative sense of the consistency of this new experimental model. The SE calculation relies on the assumption of the absence of gas-phase chemistry that was discussed in section 5.2. Consequently, only physical parameters and aqueous chemistry will be discussed as potential causes of the SE variability. In situ data on dynamics, microphysics and aqueous phase are not available. However, other quantitative indicators can be used from other platforms.

[42] A large surface monitoring network including in situ as well as remote sensors was deployed during AMMA at three mesoscale sites (150 × 150 km). Two of these sites are shown on the satellite images in Figure 4 (the Niamey and Oueme mesoscale sites). The two sites included the following instrumentation: surface rainfall gauges with a five-minute temporal resolution as part of the AMMA-CATCH program [*Lebel et al.*, 2009] and two C-band Doppler radars, respectively deployed and operated in Niamey, Niger (13.5°N, 2.2°E) by Massachusetts (USA) Institute of Technology (MIT) and Kopargo, Benin (9.8°N, 1.6°E), at the Oueme mesoscale site, by LATMOS [*Scialom et al.*, 2009], hereafter referred to as MIT and Ronsard radars. Because of the very distant radar locations, dual-Doppler analysis was not possible to derive the fine-scale wind fields. As an alternative, only mean wind profiles could be deduced from each set of single-Doppler observations. In the present study, the volume velocity processing method of *Waldteufel and Corbin* [1979] is used to obtain the mean horizontal wind components and divergence at successive regular horizontal slices (200 m and 250 m thick for Ronsard and MIT, respectively) and within a horizontal domain (60 km wide for Ronsard and 70 km for MIT) centered on the radar. Ultimately the mean vertical velocity is calculated from the upward integration of the mass continuity equation, assuming a zero vertical velocity at the surface. This vertical wind component is a key parameter as it determines the time period during which CH_2O is in contact with the liquid phase. The errors on the horizontal components and divergence are about 0.06 $m.s^{-1}$ and 1.40×10^{-5} s^{-1}. The error on the vertical velocity increases with height and could reach 0.02 and 0.05 $m.s^{-1}$ at 5 and 10 km altitude, respectively.

[43] The mass flux M_z (kg/s) of air transported vertically through a horizontal rectangular area A per unit time is expressed as [*Chong et al.*, 1987]:

$$M_z = \rho_z \times W_z \times A \tag{12}$$

where ρ_z is the air density, W_z the vertical velocity over A, at level z. Here, A equals 70×70 km^2 for the MIT radar and 60×60 km^2 for the Ronsard radar.

[44] The corresponding CH_2O mass flux is expressed as:

$$M_{CH2O} = W_z \times A \times [CH_2O]_z \tag{13}$$

where $[CH_2O]_z$ is the in situ mass concentration ($kg.m^{-3}$) of formaldehyde at the reference level z.

[45] The net vertical mass flux F_z (kg/s) can be calculated as the differential mass transport between 2 horizontal surfaces A separated by a vertical height Δz:

$$F_z(z + \Delta z/2) = M_z(z) - M_z(z + \Delta z). \tag{14}$$

[46] Positive (negative) values of F_z indicate a net vertical convergence (divergence). According to the mass equation conservation, a vertical flux convergence can be interpreted as a horizontal flux divergence. In the following, the calculated quantity $-F_z$ will be considered and termed as the horizontal flux convergence (divergence) if positive (negative).

[47] The MCSs of concern are spatially well defined as seen from the satellite images (Figure 4). Two of the four explored MCS during flights 15/08/2006b and 06/08/2006 passed through the Oueme and Niamey mesoscale sites, respectively (Figure 4). They are associated with low and high SE, respectively (Table 2). Time series of rainfall amount (Figure 5) and the vertical profiles of W_z, $-F_z$ and M_{CH2O} (Figure 6) of both MCS are examined. For the latter, only the radar sequences sounding the convective region have been considered: 7:51–9:00 A.M. for MIT (06/08/2006) and 1:38–3:06 P.M. for Ronsard (15/08/2006). M_{CH2O} is estimated from the median vertical profile of airborne CH_2O concentrations.

[48] The MCS passage explains 100% of the precipitation amount (Figure 5). Flight tracks downwind of the MCS, at and around 12 km altitude, were all performed at the end of the precipitation event. Precipitation time series show the great spatial variability of rainfall at the meso-scale. The

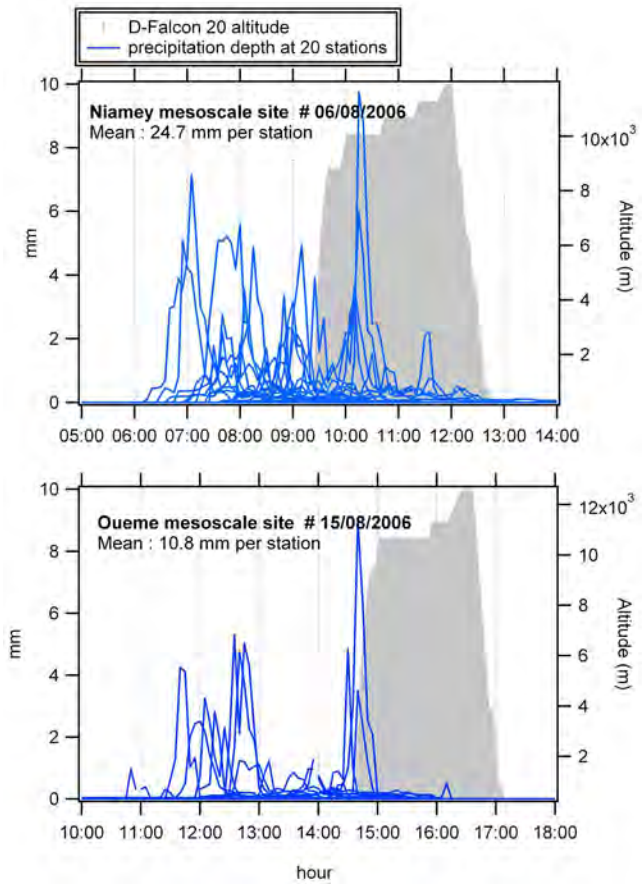

Figure 5. Time series of the precipitation depth observed at the Niamey and Oueme mesoscale sites during the passage of 2 MCS. The gray area is the altitude of the D-Falcon20 flight downwind of the MCS.

average rainfall depth is 24.7 mm in Niamey and 10.8 mm in Oueme. These equate to respective rainfall rates of 7.0 mm/h and 4.6 mm/h given the duration of each rainfall event.

[49] At all times, the vertical velocity W_z and, consequently, the convective mass flux of M_{CH2O}, are positive indicating a general upward mass transport by both MCS (Figure 6). From 4 km to 10 km, the Oueme MCS shows the highest average vertical velocity W_z, by a factor of 2, despite its greater standard deviation. The mass fluxes of CH_2O of both MCS are similar below 6 km within the standard deviations; the mass flux of CH_2O is higher between 6 km and 10 km for the Oueme MCS indicating greater transport efficiency at these levels. In general, $-F_z$ is negative above the boundary layer for the Niamey MCS and close to zero or positive for the Oueme MCS. For the former, the negative values of $-F_z$ indicates detrainment to the environment; for the latter, the positive values of $-F_z$ indicates entrainment of environmental air in the upper part of the cloud highlighting again its greater transport efficiency. By combining the previous information on rainfall rates, vertical profiles of updraft velocities and transport efficiencies (M_z and $-F_z$), it is expected that the MCS on August 6th (high SE) that passed over Niamey is more efficient in scavenging CH_2O than the MCS on August 15th that passed over Oueme (low SE). Indeed, its associated rainfall rates were about 2 times higher and updraft velocities and mass fluxes 2 times lower. This general feature is consistent with the calculated scavenging efficiency values.

[50] Given the lack of data on aqueous chemistry or condensate profiles, their respective importance on CH_2O scavenging efficiency remains uncertain but cannot be excluded [*Barth et al.*, 2007a, 2007b]. The MCS of low SE over Oueme developed over a biogenic environment. The aqueous chemistry of formaldehyde could be affected by the different availability of other water soluble VOC precursors. In the tropical forest region of Oueme, higher mixing ratios of isoprene and its oxidation products (methylvinylketone and methacrolein) were observed [*Murphy et al.*, 2010]. On the basis of observations in Amazonia [*Karl et al.*, 2004] and Malaysia [*Langford et al.*, 2010], the presence of additional oxygenated compounds of biogenic origin can be also expected in the Oueme region. These compounds are generally water soluble and can therefore be incorporated into the water cloud matrix and be oxidized by OH as efficiently as formaldehyde, their k_{OH} in the aqueous phase being in the same order of magnitude (10^8-10^9 $M^{-1}.s^{-1}$) [*Monod et al.*, 2005]. These compounds compete with formaldehyde toward reaction with OH in the aqueous phase. This process ultimately leads to less formaldehyde scavenged that would be consistent with the lower SE value for the Oueme MCS. Besides, several rainwater samples were collected at the Banizoumbou supersite (60 km east of Niamey) during seven convective events in June 2006, during the monsoon onset period in West Africa preceding SOP2-a2. The measured pH varied between 4.7 and 5.5 [*Desboeufs et al.*, 2010]. Within this larger range of pH, one could expect CH_2O scavenging efficiency to be modulated. However, this range in pH is not expected to explain the order of magnitude of differences in SE between the two MCS of interest and remains within the uncertainty on SE calculation.

6. Formaldehyde Budget and Photochemistry Downwind of MCS Over West Africa

[51] The objective of this section is to: (1) explore the chemistry of formaldehyde downwind of convection in the tropical UT of West Africa and in particular the sensitivity of formaldehyde to its gaseous precursors and (2) quantify the post-convective production of ozone and HOx radicals by testing whether or not convected formaldehyde over West Africa is a significant source of HOx and ozone in the UT.

[52] Initial mixing ratios for the base run (i.e., convective UT outflow) and background (i.e., non-convective UT air) scenarios are the mean observations collected during AMMA SOP2-a2 by the 2 French and German Falcon 20 aircraft during convective flights when available. In particular, NMHC concentrations are the ones collected on-board the F-F20 during the 4 convective events described in detail by *Bechara et al.* [2010]. Initial mixing ratios are reported in Table 3 for the different scenarios.

6.1. Model Setup

6.1.1. Treatment of Dilution and Model Evaluation

[53] The dilution rate of the convective box with the background box is constrained by CO observations, following the approach by *Bertram et al.* [2007]. The model is

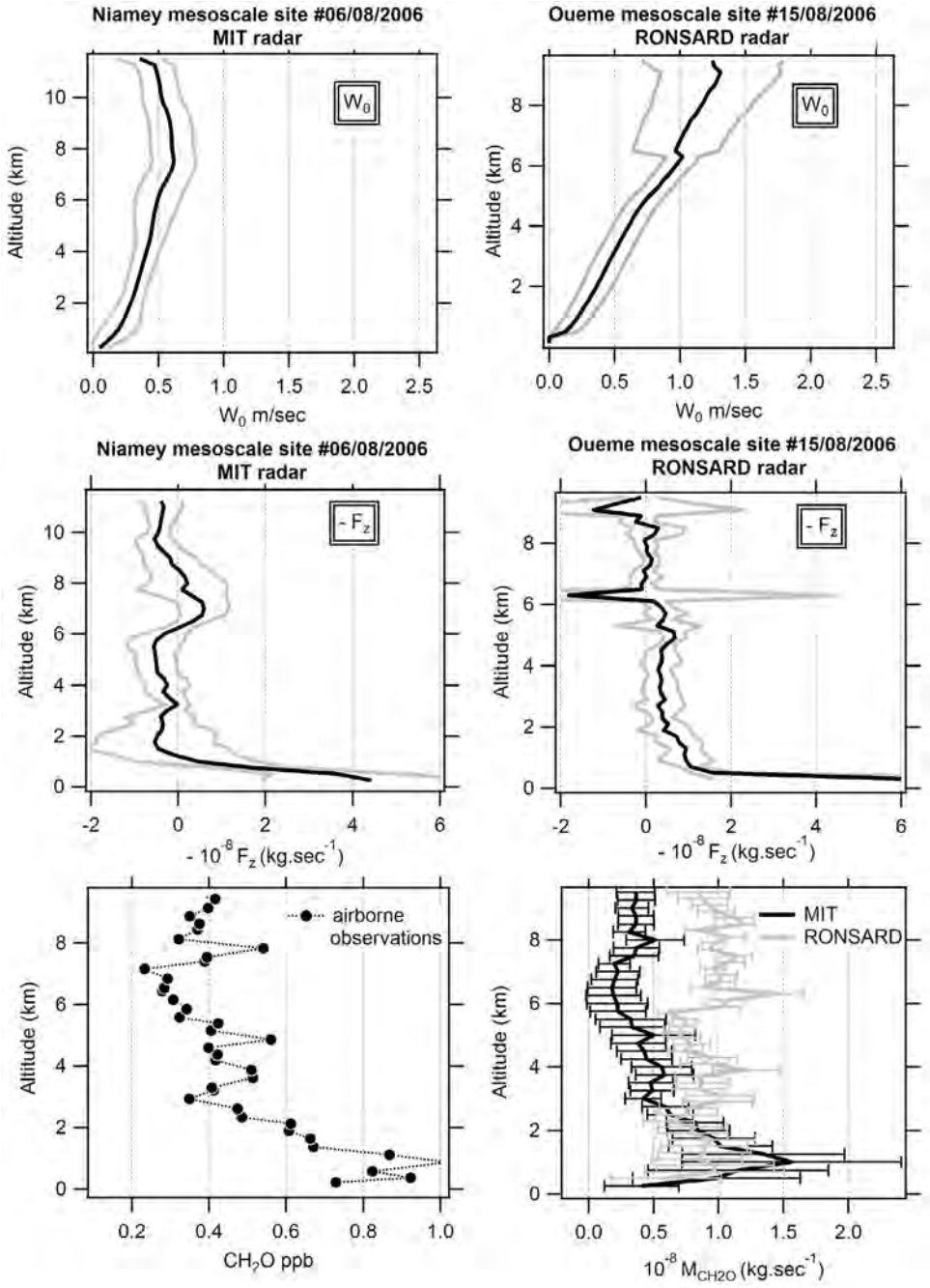

Figure 6. Vertical profiles of (top) wind vertical component W_z, (middle) differential air mass flux -Fz, and (bottom) CH_2O median mixing ratios and corresponding CH_2O mass flux of (Mz) for the Niamey and Oueme MCS scanned by the MIT and Ronsard radar, respectively. For W_z and –Fz, the black line is the average and the gray lines are average $\pm$ the standard deviation over the six sequences.

run for several dilution rates from 5% to 120% day^{-1}. The proper dilution rate is the one for which simulated CO mixing ratios match observed CO mixing ratios. The age of the outflow after convection is estimated to compare the model with observations. This time is defined as the time between the top of the convective cell and the time of the measurement. For rather fresh outflow (<15 h), the MSG-IR satellite images are overlaid with the D-Falcon 20 flight tracks by assuming that the outflow remains in a rather stationary position within the first hours (i.e., the outflow velocity is similar to the velocity of the MCS). For time > 15 h, we use a combined analysis of MSG-IR satellite images and trajectory calculation. The trajectories are calculated backward from starting points set along the D-Falcon-20 flight tracks using the Lagrangian analysis tool LAGRANTO [*Wernli and Davies*, 1997]. The wind field is retrieved from the operational archive of the ECMWF. The input data have a horizontal resolution of 0.5° × 0.5° and a vertical resolution of 91 levels. MSG-IR satellite images are overlaid with the back-trajectories and the air mass transport pathway is

Table 3. Initial Mixing Ratios of Trace Gases for the Different Simulated Scenarios[a]

	Base Run	Background	Only CH_2O	Only CH_2O Precursors	No Precursors	High NOx	Low NOx	Low VOC	High VOC	Reference
Compounds	$[X]_{CONV}$	$[X]_{UT}$	$[X]_{CONV}$	$[X]_{CONV}$		$[X]_{CONV}$	$[X]_{CONV}$	$[X]_{CONV}$	$[X]_{CONV}$	
O_3 ppb	40	50								
CO ppb	150	100								
NO	75	55				S[b]	S[c]			
NO_2	400	150				S[b]	S[c]			
PAN[d]	200	100								*Bertram et al.* [2007]
Methane[d] (ppm)	1.79	1.78	0		0[e]					*Bertram et al.* [2007]
Formaldehyde	500	170		0	0			328	1312	
Isoprene	80	50	0		0[e,f]			39	156	
Trans-2-pentene	230	15	0					114	457	
Pentane	10	5	0					4	17	
Isopentane	380	250						190	760	
Benzene	65	50	0					32	127	
Hexane	250	100	0					124	497	
Heptane	80	55	0					38	113	
Octane	120	50	0					59	235	
Toluene	165	100	0					81	325	
Ethylbenzene	180	140	0					89	355	
mp-xylene	355	250	0					175	703	
o-xlene	60	40	0					28	113	
1,2,3-TMB[g]	45	20	0					21	84	
1,2,4-TMB[g]	130	110	0					64	255	
1,3,5-TMB[g]	90	50	0					43	170	
Methanol[d]	1700	1200	0		0[h]					
Methyl hydro peroxide[d]	600	214	0		0[h]					*Ancellet et al.* [2009]
Acetone[d]	1250	1000	0		0[h]					*Murphy et al.* [2010]
H_2O_2[d]	400	500								*Ancellet et al.* [2009]

[a]All mixing ratios are in ppt except when indicated. When mixing ratios are omitted (blank entry) the values for $[X]_{conv}$ are the same as for the base run.
[b]The sum of NO and NO2 is 800.
[c]The sum of NO and NO2 is 200.
[d]Mixing ratios in the literature (see Reference entry).
[e]*No methane and isoprene* scenario.
[f]*No isoprene* scenario.
[g]TMB: trimethylbenzene.
[h]*No OVOC* scenario.

followed backward until the first encounter with a MCS as indicated by the satellite imagery. The time between the observation and the encounter of the air masses with a MCS is used to estimate the outflow age. The error in the estimation of the outflow age is 30% [*Stohl et al.*, 1998; *Harris et al.*, 2005]. The outflow age is equivalent to the time since the last convective event. Therefore, observed and simulated mixing ratios of CO and ozone can be plotted as a function of time and compared (Figure 7).

[54] The proper dilution rate is 120% day^{-1}, i.e., a dilution timescale of 20 h (Figure 7a). That is, after 20 h, the convective plume is similar to background air. It is in good agreement with the dilution timescale of 20–30 h determined by *McCormack et al.* [2000] for marine convection over the Pacific Ocean. However, the dilution rate is much higher than the 5% day^{-1} estimated by *Bertram et al.* [2007] for continental convection over northern continental midlatitudes. This elevated value highlights the strong turbulent mixing in the near field of the convection over West Africa. Over the course of 3 days, the convective plume does not remain isolated from the background UT. However, some individual convective plumes may mix at a slower rate as suggested by a few individual flights (i.e., 15th of August). The effect of a lower dilution rate on the chemical evolution of formaldehyde and photooxidant production within the convective plume will therefore be discussed.

[55] The ability of the model to reproduce photochemistry in the convective plume is evaluated by comparing simulated ozone to observed ozone mixing ratios (Figure 7b). The initial mixing ratio of ozone for the base run (40 ppb) is lower than the one of the background UT (50 ppb). This is explained by the transport of low-ozone-mixing ratio air masses from the boundary layer and free troposphere into the UT [*Bechara et al.*, 2010; *Huntrieser et al.*, 2011]. Both model and observations show an increase in ozone mixing ratios, indicating efficient ozone production downwind of MCS. During the first day after convection, observed and simulated ozone concentrations in the convective air consistently increase at a fast rate of 10 ppb day^{-1}. From the second day, the simulated ozone production slows down (3 ppb day^{-1}) while observations suggest higher values. After 48 h, the ozone reaches its photo-stationary state. Given the few observations available at outflow ages greater than 24 h and their large variability, the model is considered to provide fairly consistent results during the first 48 h after convection. These production rates are in agreement with those obtained from another AMMA modeling study [*Andres-Hernandez et al.*, 2009] but higher than other studies [*Miyazaki et al.*, 2002; *Bertram et al.*, 2007]. These results are also consistent with those of *Bertram et al.* [2007] as part of INTEX-NA over North America, which showed that low-level air masses transported by deep convection contain less ozone than UT air masses but rapid changes in

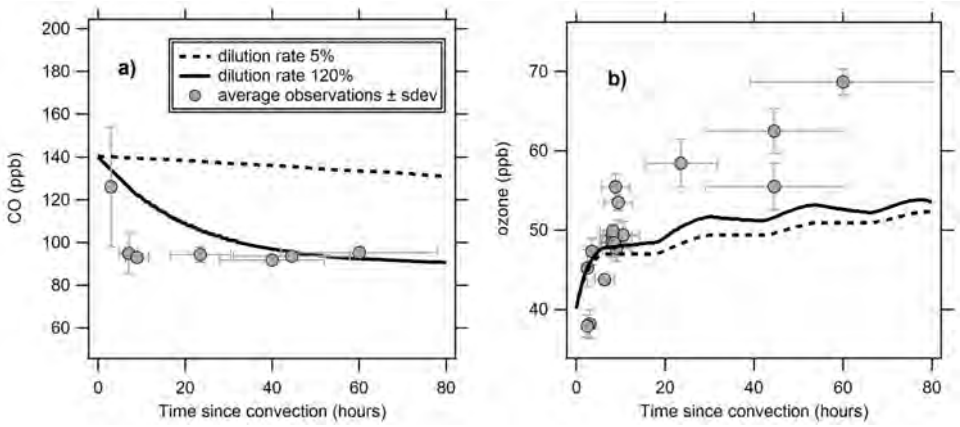

Figure 7. Temporal comparison of (a) CO and (b) ozone mixing ratios from the 0D-model and airborne observations in the convective outflow (average conditions).

ozone concentrations are observed within 2 days following the convective event.

6.1.2. Scenarios

[56] Eight scenarios of varying initial chemical composition are considered (Table 3). The *Only CH_2O* and *Only CH_2O precursors* scenarios define the direct injection of formaldehyde without any other VOCs and of all VOC precursors without formaldehyde. The *No precursors* scenario excludes the direct injection of formaldehyde and other VOC precursors: isoprene (scenario a), isoprene and methane (scenario b) and oxygenated VOC (scenario c). In each scenario, the initial mixing ratios of excluded species are set to zero in the convective UT. These scenarios test the relative importance of directly injected formaldehyde and its precursors in the production of formaldehyde and photooxidants in the UT downwind of convection. The *High and Low NOx* scenarios test the importance of injected NOx in the formaldehyde and photooxidant production in the UT downwind of convection: the initial NOx mixing ratios in the base run are set to 800 and 200 ppt, respectively. The *High and Low VOC* scenarios test the importance of injected VOC in the formaldehyde and photooxidant production in the UT downwind of convection. The *low-VOC* and *high-VOC* cases correspond to a β value of 0.2 and 0.8, respectively, from uplifted boundary layer.

6.2. Formaldehyde Downwind of MCS Over West Africa

[57] Injected formaldehyde is quickly depleted within a few hours (Figure 8a, *only CH_2O scenario*). The most important destruction terms of formaldehyde in the UT are its reaction with OH and photolysis. Based on the comparison between the *only CH_2O precursors* scenario and the *base run* scenario, the secondary formation of CH_2O from injected VOC precursors is the dominant source of formaldehyde in the UT after convection, in agreement with *Fried et al.* [2008b] who found that ~70% of the convectively perturbed UT air originated from CH_2O precursors. This result also suggests that the SE previously determined (section 5.5) should be seen as a lower limit. Anthropogenic NMHC are the major CH_2O precursors in the convective outflow plume of West Africa when comparing the different *no precursors* scenarios with the *only CH_2O precursors* one: 80% of secondary CH_2O is explained by anthropogenic NMHC. Formaldehyde mixing ratios are sensitive to the initial VOC precursor loads during the first day of the simulation. After 30 h, CH_2O reaches a photo-stationary state. Similarly, the sensitivity of CH_2O to NOx initial mixing ratios is high during the first day of the simulation when comparing the *high NOx* scenarios to the *base run.* This is consistent with previous studies in the UT [*Stickler et al.*, 2006; *Fried et al.*, 2008a, 2008b] but CH_2O was still affected by NOx after one week in *Fried et al.* [2008b]. In particular, the enhanced NO due to lightning increases the reaction of methylperoxy radicals (CH_3O_2), and more generally RO_2 radicals, in forming CH_2O.

[58] The evolution of simulated CH_2O is compared to observed CH_2O from the D-Falcon 20 flights in Figure 8b. The evolution of observed and simulated CH_2O is consistent by showing a decrease of formaldehyde mixing ratios over time. Depletion processes (photolysis and OH-oxidation) dominate the fate of formaldehyde downwind of MCS over West Africa as already seen by *Fried et al.* [2008b] in the continental UT over North America. This outcome is consistent with the low sensitivity observed for CH_2O to the value of the dilution rate (not shown here). However, after 20 h, the observed CH_2O mixing ratios are 3 to 4 times higher than the simulated ones suggesting that the CH_2O depletion rate in the outflow is much lower than suggested by the model. These discrepancies imply one or a combination of the following hypothesis: (1) additional unknown source of CH_2O hydrocarbon precursors and higher NO, (2) modeled CH_2O sink terms that are too fast compared with reality. Regarding the first potential cause, the *high-NOx* scenario does reduce the gap between the model and observations (Figure 8b). A NO-dependent discrepancy between modeled/observed CH_2O and HO_2 in the continental UT (10–12 km) during INTEX-NA was depicted by *Fried et al.* [2008b], However, the maximum mixing ratios of NO observed during AMMA hardly exceeded 1.5 ppb [*Huntrieser et al.*, 2011] and are not expected to fully explain a difference of a factor 3–4. The second potential cause can be seen as a source of uncertainty as the model only considers the gas phase chemistry in cloud-free conditions and uses modeled photolysis rates. Therefore, the enhancement or reduction in the radiation field due to cloud

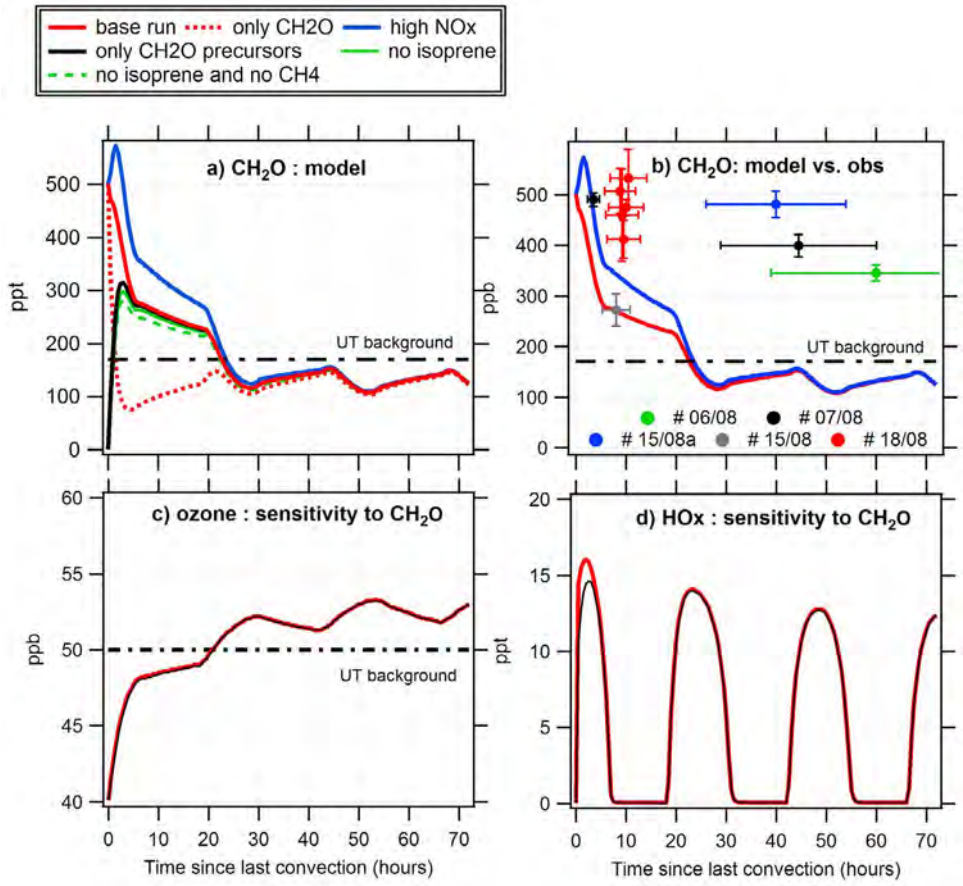

Figure 8. Time dependent simulation of trace gas evolution in MCS outflow over West Africa: (a) CH_2O, (b) CH_2O compared with airborne observations, (c) ozone, and (d) HOx. Airborne CH_2O observations (Figure 9b) are given by the colored dots with the uncertainty limits on both time and concentration axis. The horizontal black dotted lines are the mixing ratio of background formaldehyde or ozone in the dilution box. Color codes apply for all plots.

impacts is not accounted in the model. In particular, it was estimated in section 5.2 that the lifetime of formaldehyde with respect to photolysis is increased to 8 h within the cloud (versus 1.5 h in cloud-free conditions). Therefore, the intensity of the solar radiation in the model can be seen as a major cause of discrepancy between observed and simulated formaldehyde.

[59] Finally, as seen from Figures 8c and 8d, ozone production as well as HOx production in the convective UT is not sensitive to formaldehyde that is directly injected by convection when comparing the *base run* with the *only CH_2O precursors* run.

6.3. Photooxidant Production Downwind of MCS Over West Africa

[60] The ozone concentrations vary with initial NOx levels (Figure 9a) which characterizes a NOx-limited regime. The higher the NOx levels are, the higher the ozone levels are and the faster the ozone production is, especially during the first 20 h of the simulation. After one day, ozone reaches its photo-stationary state. Conversely, ozone production is not sensitive to the VOC initial loads (Figure 9b). Finally, the chemistry of the convective plume in term of ozone production is only efficient during the first 20 h after convection given the high dilution rate.

[61] The effect of a lower dilution rate on the ozone production is shown in Figure 9c and 9d. At a low dilution rate (5%), the ozone production is maintained over the course of 3 days and varies widely with NOx levels as seen from the *base run* and *high-NOx* scenario in Figure 9c. While ozone production is NOx-limited in convective UT, the initial VOC loads also modulate its production after one day (Figure 9c). Surprisingly, the *low-VOC* ozone is higher than the *high-VOC* ozone at the end of the simulation (+11%). In the *low-VOC* scenario, the ozone production rate is three times higher than in the *high VOC* scenario. The temporal evolution of NOy species for *low-VOC* and *high-VOC* scenarios is reported in Figure 9d. The simulation shows that the increase of the initial VOC loads leads to a higher production of nitrogen-containing organic species (organic nitrates and PAN like compounds). This enhanced production of these nitrogen reservoirs reduces the amount of NOx available. With ozone production being NOx-limited in the UT, increasing the amount of VOC injected ultimately leads to a decrease in ozone production rate.

[62] From these simulations, it appears that the dilution rate controls the importance of ozone production downwind

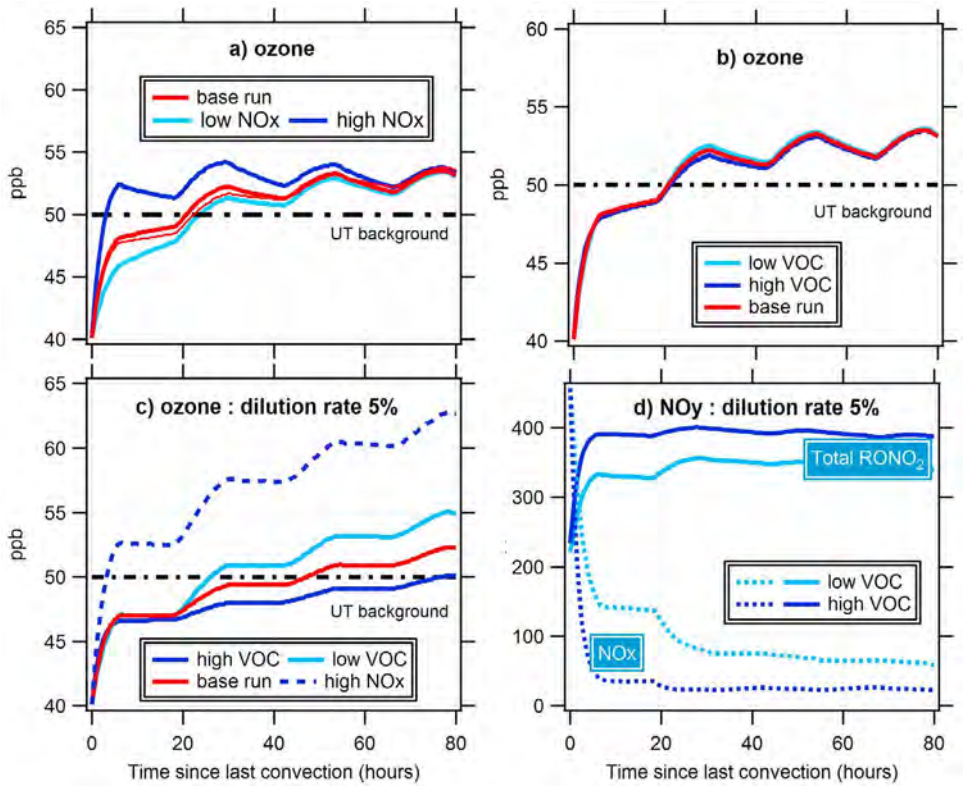

Figure 9. Time dependent simulation of ozone and NOy evolution in MCS outflow over West Africa under different scenarios regarding (a) NOx, (b) VOC, (c) dilution rate and (d) VOC at a low dilution rate of 5%.

of MCS. At high dilution rate (from 75% day^{-1}), the downwind production of ozone is inefficient. However, at lower dilution rate, ozone production is then sensitive to its gaseous precursors. While the ozone production is NOx-limited, it is also critical to accurately estimate the amount of VOC precursors injected into the UT and especially the highly reactive isoprene, which is expected to be important over forested tropical regions. Indeed, the recent study by *Emmerson and Evans* [2009] has shown that the impact of isoprene on the production of O_3 can vary enormously depending on the treatment of the isoprene nitrates in the chemical scheme, in particular whether they act as a sink for NOx or recycle it.

7. Conclusion

[63] A unique comprehensive and consistent data set of formaldehyde mixing ratios was constructed to examine the impact of tropical continental deep convection on formaldehyde over West Africa. In particular, the multiple aircraft strategy deployed during the AMMA experiment in summer 2006 provided a 3-D-spatially resolved formaldehyde data set in various conditions including the boundary, free and upper troposphere layers in background and convective conditions.

[64] A new three-component mixture model based on formaldehyde and other trace gases observations (CO and VOC) was developed to estimate the scavenging efficiency of formaldehyde by deep convection. This new model showed that the fraction of free tropospheric air from mid-levels in the fresh convective outflow is close to 50% and cannot be neglected in the calculation of the scavenging efficiency. As a consequence, the commonly used two component mixture model, which only takes into account the contribution of the boundary layer air, is not appropriate. This result is also helpful for the setup of future aircraft campaigns exploring the impact of deep convection on the chemical composition of the upper troposphere. Indeed, information on the free troposphere composition is another key observational constraint to estimate the impact of deep convection on the redistribution of reactive species.

[65] During convective transport, the photochemical production of formaldehyde by its uplifted VOC precursors could be significant while its photochemical depletion is small. This secondary production counterbalances its loss uptake into the cloud matrix represented by the scavenging efficiency term (SE), and hence our SE determinations may be lower limits. The scavenging efficiency of formaldehyde by the convective cloud is highly variable within an order of magnitude among the studied MCS (4% to 40%). The variability of the SE could be, at least, explained by the differences between MCS features: rainfall depth, vertical wind velocity and mass fluxes that were derived from the rainfall gauges and Doppler radar networks at the ground.

[66] A 0-D time dependent photochemical box model was applied to convective UT air. The dilution rate of the convective air was estimated to be high downwind of MCS developing over West Africa with a characteristic mixing time of 20 h. After convection, most of the formaldehyde in the UT is photochemically produced by its anthropogenic

VOC precursors that are uplifted from the boundary and intermediate layers, in agreement with *Fried et al.* [2008b]. Then, formaldehyde is depleted, as also seen from the observations. Finally, formaldehyde directly injected by convection does not impact ozone and HOx production in the tropical UT of West Africa. While the production of ozone in post-convective UT is NOx-sensitive, the dilution rate and, as a consequence, the amount of injected VOCs, also modulate the ozone production through the conversion of NOx into PAN and other organic nitrates. Previous modeling studies have shown that the impact of isoprene on ozone in the UT is highly variable depending on the treatment of the isoprene nitrates in the chemical scheme. Therefore, it is important to put efforts into the quantification of isoprene and other organic nitrates transported by deep convection in future studies that will address the impact of deep convection on UT chemistry. In particular, this will be of great importance over forested tropical regions. This will help in a better understanding of the isoprene chemistry as well as the role of organic nitrates in transporting reactive nitrogen far from their source region.

[67] **Acknowledgments.** Based on a French initiative, AMMA was built by an international scientific group and is currently funded by a large number of agencies, especially from France, the United Kingdom, the United States, and Africa. It has been the beneficiary of a major financial contribution from the European Community Sixth Framework Research Programme. Detailed information on scientific coordination and funding is available on the AMMA International Web site at http://www.amma-international.org. Agnès Borbon was partly funded by the CIRES Visiting Fellow Program. Special thanks are due to the English, French and German aircraft operators and Earle Williams and Bryan Russell who kindly put the MIT Doppler radar data collected during AMMA at the disposal of the scientific community. Timothy Bertram, Ron Cohen and Paul Monks are thanked for providing the INTEX-NA model initialization data and the j(NO_2) data. Discussions at the beginning of this work with Mary Barth, Eric Apel and Chris Cantrell at NCAR and the Tropospheric Chemistry Group at the Chemical Science Division at NOAA (Boulder, USA) were appreciated. We are grateful to Alan Fried (NCAR) for his detailed comments on the manuscript. Finally, the authors would like to thank the anonymous reviewers for their comments to improve the quality of the manuscript.

References

Ancellet, G., J. L. de Bellevue, C. Mari, P. Nedelec, A. Kukui, A. Borbon, and P. Perros (2009), Effects of regional-scale and convective transports on tropospheric ozone chemistry revealed by aircraft observations during the wet season of the AMMA campaign, *Atmos. Chem. Phys.*, *9*(2), 383–411, doi:10.5194/acp-9-383-2009.

Andres-Hernandez, M. D., D. Kartal, L. Reichert, J. P. Burrows, J. Meyer Arnek, M. Lichtenstern, P. Stock, and H. Schlager (2009), Peroxy radical observations over West Africa during AMMA 2006: Photochemical activity in the outflow of convective systems, *Atmos. Chem. Phys.*, *9*, 3681–3695.

Atkinson, R. (2000), Atmospheric chemistry of VOCs and NOx, *Atmos. Environ.*, *34*, 2063–2101, doi:10.1016/S1352-2310(99)00460-4.

Barth, M. C., S. W. Kim, W. C. Skamarock, A. L. Stuart, K. E. Pickering, and L. E. Ott (2007a), Simulations of the redistribution of formaldehyde, formic acid, and peroxides in the 10 July 1996 Stratospheric-Tropospheric Experiment: Radiation, Aerosols, and Ozone deep convection storm, *J. Geophys. Res.*, *112*, D13310, doi:10.1029/2006JD008046.

Barth, M. C., et al. (2007b), Cloud-scale model intercomparison of chemical constituent transport in deep convection, *Atmos. Chem. Phys.*, *7*(18), 4709–4731, doi:10.5194/acp-7-4709-2007.

Barthe, C., C. Mari, J. P. Chaboureau, P. Tulet, and J. P. Pinty (2011), Numerical study of tracers transport by mesoscale convective systems over West Africa, *Ann. Geophys.*, *29*, 731–747, doi:10.5194/angeo-29-731-2011.

Bechara, J., A. Borbon, C. Jambert, and P. E. Perros (2008), New off-line aircraft instrumentation for non-methane hydrocarbon measurements, *Anal. Bioanal. Chem.*, *392*, 865–876, doi:10.1007/s00216-008-2330-3.

Bechara, J., A. Borbon, C. Jambert, A. Colomb, and P. E. Perros (2010), Evidence of the impact of deep convection on reactive Volatile Organic Compounds in the upper tropical troposphere during the AMMA experiment in West Africa, *Atmos. Chem. Phys.*, *10*, 10,321–10,334, doi:10.5194/acp-10-10321-2010.

Bertram, T. H., et al. (2007), Direct measurements of the convective recycling of the upper troposphere, *Science*, *315*, 816–820, doi:10.1126/science.1134548.

Blake, N. J., D. R. Blake, B. C. Sive, T.-Y. Chen, F. S. Rowland, J. E. Collins Jr., G. W. Sachse, and B. E. Anderson (1996), Biomass burning emissions and vertical distribution of atmospheric methyl halides and other reduced carbon gases in the South Atlantic region, *J. Geophys. Res.*, *101*, 24,151–24,164, doi:10.1029/96JD00561.

Borrmann, S., et al. (2010), Aerosols in the tropical and subtropical UT/LS: In-situ measurements of submicron particle abundance and volatility, *Atmos. Chem. Phys.*, *10*(12), 5573–5592, doi:10.5194/acp-10-5573-2010.

Cárdenas, L. M., D. J. Brassington, B. J. Allan, H. Coe, B. Alicke, U. Platt, K. M. Wilson, J. M. C. Plane, and S. A. Penkett (2000), Intercomparison of formaldehyde measurements in clean and polluted atmospheres, *J. Atmos. Chem.*, *37*(1), 53–80, doi:10.1023/A:1006383520819.

Carlier, P., H. Hannachi, and G. Mouvier (1986), The chemistry of carbonyl compounds in the atmosphere—A review, *Atmos. Environ.*, *20*(11), 2079–2099, doi:10.1016/0004-6981(86)90304-5.

Chong, M. (2011), The 11 August 2006 squall-line system as observed from MIT Doppler radar during the AMMA SOP, *Q. J. R. Meteorol. Soc.*, *139*(1), 209–226.

Chong, M., P. Amayenc, G. Scialom, and J. Testud (1987), A tropical squall line observed during the COPT 81 experiment. Part I: Kinematic structure inferred from dual-Doppler radar data, *Mon. Weather Rev.*, *115*, 670–694, doi:10.1175/1520-0493(1987)115<0670:ATSLOD>2.0.CO;2.

Cohan, D. S., M. G. Schultz, D. J. Jacob, B. G. Heikes, and D. R. Blake (1999), Convective injection and photochemical decay of peroxides in the tropical upper troposphere: Methyl iodide as a tracer of marine convection, *J. Geophys. Res.*, *104*(D5), 5717–5724, doi:10.1029/98JD01963.

Colomb, A., et al. (2006), Airborne measurements of trace organic species in the upper troposphere over Europe: The impact of deep convection, *Environ. Chem.*, *3*(4), 244–259, doi:10.1071/EN06020.

Commane, R., C. F. A. Floquet, T. Ingham, D. Stone, M. J. Evans, and D. E. Heard (2010), Observations of OH and HO_2 radicals over West Africa, *Atmos. Chem. Phys.*, *10*, 8783–8801, doi:10.5194/acp-10-8783-2010.

Desboeufs, K., E. Journet, J.-L. Rajot, S. Chevaillier, S. Triquet, P. Formenti, and A. Zakou (2010), Chemistry of rain events in West Africa: Evidence of dust and biogenic influence in convective systems, *Atmos. Chem. Phys.*, *10*, 9283–9293, doi:10.5194/acp-10-9283-2010.

Doherty, R. M., D. S. Stevenson, W. J. Collins, and M. J. Sanderson (2005), Influence of convective transport on tropospheric ozone and its precursors in a chemistry-climate model, *Atmos. Chem. Phys.*, *5*, 3205–3218, doi:10.5194/acp-5-3205-2005.

Duane, M., B. Poma, D. Rembges, C. Astorga, and B. R. Larsen (2002), Isoprene and its degradation products as strong ozone precursors in Insubria, northern Italy, *Atmos. Environ.*, *36*, 3867–3879, doi:10.1016/S1352-2310(02)00359-X.

Emmerson, K. M., and M. J. Evans (2009), Comparison of tropospheric gas-phase chemistry schemes for use within global models, *Atmos. Chem. Phys.*, *9*, 1831–1845, doi:10.5194/acp-9-1831-2009.

Folkins, I., and R. Chatfield (2000), Impact of acetone on ozone production and OH in the upper troposphere at high NO_x, *J. Geophys. Res.*, *105*(D9), 11,585–11,599, doi:10.1029/2000JD900067.

Fried, A., Y.-N. Lee, G. Frost, B. Wert, B. Henry, J. R. Drummond, G. Hübler, and T. Jobson (2002), Airborne CH_2O measurements over the North Atlantic during the 1997 NARE campaign: Instrument comparisons and distributions, *J. Geophys. Res.*, *107*(D4), 4039, doi:10.1029/2000JD000260.

Fried, A., et al. (2008a), Formaldehyde over North America and the North Atlantic during the summer 2004 INTEX campaign: Methods, observed distributions, and measurement-model comparisons, *J. Geophys. Res.*, *113*, D10302, doi:10.1029/2007JD009185.

Fried, A., et al. (2008b), Role of convection in redistributing formaldehyde to the upper troposphere over North America and the North Atlantic during the summer 2004 INTEX campaign, *J. Geophys. Res.*, *113*, D17306, doi:10.1029/2007JD009760.

Gilpin, T., et al. (1997), Intercomparison of six ambient [CH_2O] measurement techniques, *J. Geophys. Res.*, *102*, 21,161–21,188, doi:10.1029/97JD01314.

Guenther, A., et al. (1995), A global model of natural volatile organic compound emissions, *J. Geophys. Res.*, *100*(D5), 8873–8892, doi:10.1029/94JD02950.

Hak, C., et al. (2005), Intercomparison of four different in-situ techniques for ambient formaldehyde measurements in urban air, *Atmos. Chem. Phys.*, *5*, 2881–2900, doi:10.5194/acp-5-2881-2005.

Harris, J. M., R. R. Draxler, and S. J. Oltmans (2005), Trajectory model sensitivity to differences in input data and vertical transport method, *J. Geophys. Res.*, *110*, D14109, doi:10.1029/2004JD005750.

Homan, C. D., C. M. Volk, A. C. Kuhn, A. Werner, J. Baehr, S. Viciani, A. Ulanovski, and F. Ravegnani (2010), Tracer measurements in the tropical tropopause layer during the AMMA/SCOUT-O3 aircraft campaign, *Atmos. Chem. Phys.*, *10*(8), 3615–3627, doi:10.5194/acp-10-3615-2010.

Houze, R. A. (1989), Observed structure of mesoscale convective systems and implications for large scale heating, *Q. J. R. Meteorol. Soc.*, *115*(487), 425–461, doi:10.1002/qj.49711548702.

Huntrieser, H., et al. (2011), Mesoscale convective systems observed during AMMA and their impact on the NOx and O_3 budget over West Africa, *Atmos. Chem. Phys.*, *11*, 2503–2536, doi:10.5194/acp-11-2503-2011.

Jaeglé, L., et al. (1997), Observed OH and HO_2 in the upper troposphere suggest a major source from convective injection of peroxides, *Geophys. Res. Lett.*, *24*(24), 3181–3184, doi:10.1029/97GL03004.

Jaeglé, L., D. J. Jacob, W. H. Brune, D. Tan, I. C. Faloona, A. J. Weinheimer, B. A. Ridley, T. L. Campos, and G. W. Sachse (1998), Sources of HO_x and production of ozone in the upper troposphere over the United States, *Geophys. Res. Lett.*, *25*(10), 1709–1712, doi:10.1029/98GL00041.

Janicot, S., et al. (2008), Large-scale overview of the summer monsoon over West Africa during the AMMA field experiment in 2006, *Ann. Geophys.*, *26*(9), 2569–2595, doi:10.5194/angeo-26-2569-2008.

Jenkin, M. E., S. M. Saunders, V. Wagner, and M. J. Pilling (2003), Protocol for the development of the Master Chemical Mechanism, MCM v3 (Part B): Tropospheric degradation of aromatic volatile organic compounds, *Atmos. Chem. Phys.*, *3*, 181–193, doi:10.5194/acp-3-181-2003.

Junkermann, W., and J. M. Burger (2006), A new portable instrument for continuous measurements of formaldehyde in ambient air, *J. Atmos. Oceanic Technol.*, *23*, 38–45, doi:10.1175/JTECH1831.1.

Karl, T., M. Potosnak, A. Guenther, D. Clark, J. Walker, J. D. Herrick, and C. Geron (2004), Exchange processes of volatile organic compounds above a tropical rain forest: Implications for modeling tropospheric chemistry above dense vegetation, *J. Geophys. Res.*, *109*, D18306, doi:10.1029/2004JD004738.

Kormann, R., et al. (2003), Formaldehyde over the eastern Mediterranean during MINOS: Comparison of airborne in-situ measurements with 3D-model results, *Atmos. Chem. Phys.*, *3*, 851–861, doi:10.5194/acp-3-851-2003.

Kraus, A., and A. Hofzumahaus (1998), Field measurements of atmospheric photolysis frequencies for O_3, NO_2, HCHO, CH_3CHO, H_2O_2, and HONO by UV spectroradiometry, *J. Atmos. Chem.*, *31*(1/2), 161–180, doi:10.1023/A:1005888220949.

Lafore, J. P., et al. (2011), Progress in understanding of weather systems in West Africa, *Atmos. Sci. Lett.*, *12*, 7–12, doi:10.1002/asl.335.

Langford, B., P. K. Misztal, E. Nemitz, B. Davison, C. Helfter, T. A. M. Pugh, A. R. MacKenzie, S. F. Lim, and C. N. Hewitt (2010), Fluxes and concentrations of volatile organic compounds from a South-East Asian tropical rainforest, *Atmos. Chem. Phys.*, *10*, 8391–8412, doi:10.5194/acp-10-8391-2010.

Law, K. S., et al. (2010), Air mass origins influencing TTL chemical composition over West Africa during 2006 summer monsoon, *Atmos. Chem. Phys.*, *10*(22), 10,753–10,770, doi:10.5194/acp-10-10753-2010.

Lawrence, M. G., R. von Kuhlmann, M. Salzmann, and P. J. Rasch (2003), The balance of effects of deep convective mixing on tropospheric ozone, *Geophys. Res. Lett.*, *30*(18), 1940, doi:10.1029/2003GL017644.

Lebel, T., et al. (2009), AMMA-CATCH studies in the Sahelian region of West-Africa: An overview, *J. Hydrol.*, *375*, 3–13, doi:10.1016/j.jhydrol.2009.03.020.

Lee, Y. N., X. Zhou, R. W. Leaitch, and C. M. Barnic (1996), An aircraft measurement technique for formaldehyde and soluble carbonyl compounds, *J. Geophys. Res.*, *101*(D22), 29,075–29,080, doi:10.1029/95JD03827.

Lelieveld, J., and P. Crutzen (1991), Role of clouds in tropospheric chemistry, *J. Atmos. Chem.*, *12*, 229–267, doi:10.1007/BF00048075.

Lelieveld, J., and P. Crutzen (1994), Role of convection in the ozone budget of the upper troposphere, *Science*, *264*, 1759–1761, doi:10.1126/science.264.5166.1759.

Lelieveld, J., et al. (2002), Global air pollution crossroads over the Mediterranean, *Science*, *298*(5594), 794–799, doi:10.1126/science.1075457.

Leriche, M., D. Voisin, N. Chaumerliac, A. Monod, and B. Aumont (2000), A model for tropospheric multiphase chemistry: Application to one cloudy event during the CIME experiment, *Atmos. Environ.*, *34*, 5013–5036, doi:10.1016/S1352-2310(00)00329-0.

Lopez, J. P., et al. (2006), CO signatures in subtropical convective clouds and anvils during CRYSTAL-FACE: An analysis of convective transport and entrainment using observations and a cloud-resolving model, *J. Geophys. Res.*, *111*, D09305, doi:10.1029/2005JD006104.

Madronich, S., and F. Flocke (1998), The role of solar radiation in atmospheric chemistry, in *Handbook of Environmental Chemistry*, edited by P. Boule, pp. 1–26, Springer, New York.

Mari, C., D. J. Jacob, and P. Bechtold (2000), Transport and scavenging of soluble gases in a deep convective cloud, *J. Geophys. Res.*, *105*(D17), 22,255–22,267, doi:10.1029/2000JD900211.

Mari, C., et al. (2002), On the relative role of convection, chemistry, and transport over the South Pacific Convergence Zone during PEM-Tropics B: A case study, *J. Geophys. Res.*, *107*(D2), 8232, doi:10.1029/2001JD001466. [printed *108*(D2), 2003].

Mari, C. H., G. Cailley, L. Corre, M. Saunois, J.-L. Attié, V. Thouret, and A. Stohl, (2008), Tracing biomass burning plumes from the Southern Hemisphere during the AMMA 2006 wet season experiment, *Atmos. Chem. Phys.*, *8*(14), 3951–3961, doi:10.5194/acp-8-3951-2008.

Martin, R. V., D. J. Jacob, J. A. Logan, I. Bey, R. M. Yantosca, A. C. Staudt, Q. Li, A. M. Fiore, B. N. Duncan, and H. Liu (2002), Interpretation of TOMS observations of tropical tropospheric ozone with a global model and in situ observations, *J. Geophys. Res.*, *107*(D18), 4351, doi:10.1029/2001JD001480.

Mauldin, R. L., III, S. Madronich, S. J. Flocke, and L. Eisele (1997), New insights on OH' Measurements around and in clouds, *Geophys. Res. Lett.*, *24*(23), 3033–3036, doi:10.1029/97GL02983.

McCormack, J. P., R. Fu, and W. G. Read (2000), The influence of convective outflow on water vapor mixing ratios in the tropical upper troposphere: An analysis based on UARS MLS measurements, *Geophys. Res. Lett.*, *27*(4), 525–528, doi:10.1029/1999GL010477.

McKeen, S. A., T. Gierczak, J. B. Burkholder, P. O. Wenneberg, and T. F. Hanisco (1997), The photochemistry of acetone in the upper troposphere: A source of odd-hydrogen radicals, *Geophys. Res. Lett.*, *24*(24), 3177–3180, doi:10.1029/97GL03349.

Minga, A., V. Thouret, M. Saunois, C. Delon, D. Serça, C. Mari, B. Sauvage, A. Mariscal, M. Leriche, and B. Cros (2010), What caused extreme ozone concentrations over Cotonou in December 2005, *Atmos. Chem. Phys.*, *10*(3), 895–907, doi:10.5194/acp-10-895-2010.

Miyazaki, Y., K. Kita, Y. Kondo, M. Koike, M. Ko, W. Hu, S. Kawakami, D. R. Blake, and T. Ogawa (2002), Springtime photochemical ozone production observed in the upper troposphere over east Asia, *J. Geophys. Res.*, *108*(D3), 8398, doi:10.1029/2001JD000811.

Monks, P. S., A. R. Rickard, S. L. Hall, and N. A. D. Richards (2004), Attenuation of spectral flux and photolysis frequencies at the surface through homogenous cloud fields, *J. Geophys. Res.*, *109*, D17206, doi:10.1029/2003JD004076.

Monod, A., L. Poulain, S. Grubert, D. Voisin, and H. Wortham (2005), Kinetics of OH-initiated oxidation of oxygenated organic compounds in the aqueous phase: New rate constants, structure-activity relationships and atmospheric implications, *Atmos. Environ.*, *39*, 7667–7688, doi:10.1016/j.atmosenv.2005.03.019.

Müller, J. F., and G. Brasseur (1999), Sources of upper tropospheric HO_x: A three-dimensional study, *J. Geophys. Res.*, *104*(D1), 1705–1715, doi:10.1029/1998JD100005.

Murphy, J. G., D. E. Oram, and C. E. Reeves (2010), Measurements of volatile organic compounds over West Africa, *Atmos. Chem. Phys.*, *10*, 5281–5294, doi:10.5194/acp-10-5281-2010.

Prather, M. J., and D. J. Jacob (1997), A persistent imbalance in HO_x and NO_x photochemistry of the upper troposphere driven by deep tropical convection, *Geophys. Res. Lett.*, *24*(24), 3189–3192, doi:10.1029/97GL03027.

Raper, J. L., M. M. Kleb, D. J. Jacob, D. D. Davis, R. E. Newell, H. E. Fuelberg, R. J. Bendura, J. M. Hoell, and R. J. McNeal (2001), Pacific Exploratory Mission in the Tropical Pacific: PEM-Tropics B, March-April 1999, *J. Geophys. Res.*, *106*(D23), 32,401–32,425, doi:10.1029/2000JD900833.

Ravetta, F., et al. (2001), Experimental evidence for the importance of convected methylhydroperoxide as a source of hydrogen oxide (HO_x) radicals in the tropical upper troposphere, *J. Geophys. Res.*, *106*(D23), 32,709–32,716, doi:10.1029/2001JD900009.

Redelsperger, J.-L., C. D. Thorncroft, A. Diedhiou, T. Lebel, D. J. Parker, and J. Polcher (2006), African Monsoon Multidisciplinary Analysis: An international research project and field campaign, *Bull. Am. Meteorol. Soc.*, *87*(12), 1739–1746, doi:10.1175/BAMS-87-12-1739.

Reeves, C. E., et al. (2010), Chemical and aerosol characterisation of the troposphere over West Africa during the monsoon period as part of AMMA, *Atmos. Chem. Phys.*, *10*, 7575–7601, doi:10.5194/acp-10-7575-2010.

Sander, S. P., et al. (2011), Chemical kinetics and photochemical data for use in atmospheric studies: Evaluation number 17, *JPL Publ.*, *10-6*, 34 pp.

Saunders, S. M., M. E. Jenkin, R. G. Derwent, and M. J. Pilling (2003), Protocol for the development of the Master Chemical Mechanism, MCM v3

(Part A): Tropospheric degradation of non-aromatic volatile organic compounds, *Atmos. Chem. Phys.*, *3*, 161–180, doi:10.5194/acp-3-161-2003.

Saunois, M., C. E. Reeves, C. H. Mari, J. G. Murphy, D. J. Stewart, G. P. Mills, D. E. Oram, and R. M. Purvis (2009), Factors controlling the distribution of ozone in the West African lower troposphere during the AMMA (African Monsoon Multidisciplinary Analysis) wet season campaign, *Atmos. Chem. Phys.*, *9*(16), 6135–6155, doi:10.5194/acp-9-6135-2009.

Scialom, G., J. Faroux, M. Giraud, R. Ney, R. Evaristo, Y. Lemaître, and N. Viltard (2009), RONSARD radar: Implementation of dual polarization on a C-band Doppler weather radar, *IEEE Geosci. Remote Sens. Lett.*, *6*(1), 132–136, doi:10.1109/LGRS.2008.2008318.

Serça, D., R. Delmas, X. Le Roux, D. A. B. Parsons, M. C. Scholes, L. Abbadie, R. Lensi, O. Ronce, and L. Labroue (1998), Comparison of nitrogen monoxide emissions from several African tropical ecosystems and influence of season and fire, *Global Biogeochem. Cycles*, *12*(4), 637–651, doi:10.1029/98GB02737.

Shapiro, S. S., and M. B. Wilk (1965), An analysis of variance test for normality (complete samples), *Biometrika*, *52*, 561–610.

Sprengnether, M., K. L. Demerjian, N. M. Donahue, and J. G. Anderson (2002), Product analysis of the OH oxidation of isoprene and 1,3-butadiene in the presence of NO, *J. Geophys. Res.*, *107*(D15), 4268, doi:10.1029/2001JD000716.

Stark, H., B. M. Lerner, R. Schmitt, R. Jakoubek, E. J. Williams, T. B. Ryerson, D. T. Sueper, D. D. Parrish, and F. C. Fehsenfeld (2007), Atmospheric in situ measurement of nitrate radical (NO_3) and other photolysis rates using spectroradiometry and filter radiometry, *J. Geophys. Res.*, *112*, D10S04, doi:10.1029/2006JD007578.

Stevenson, D. S., et al. (2006), Multimodel ensemble simulations of present-day and near-future tropospheric ozone, *J. Geophys. Res.*, *111*, D08301, doi:10.1029/2005JD006338.

Stickler, A., H. Fischer, J. Williams, M. de Reus, R. Sander, M. G. Lawrence, J. N. Crowley, and J. Lelieveld (2006), Influence of summertime deep convection on formaldehyde in the middle and upper troposphere over Europe, *J. Geophys. Res.*, *111*, D14308, doi:10.1029/2005JD007001.

Still, T. J., S. Al-Haider, P. W. Seakins, R. Sommariva, J. C. Stanton, G. Mills, and S. A. Penkett (2006), Ambient formaldehyde measurements made at a remote marine boundary layer site during the NAMBLEX campaign—A comparison of data from chromatographic and modified Hantzsch techniques, *Atmos. Chem. Phys.*, *6*, 2711–2726, doi:10.5194/acp-6-2711-2006.

Stohl, A., M. Hittenberger, and G. Wotawa (1998), Validation of the Lagrangian particle dispersion model FLEXPART against large-scale tracer experiment data, *Atmos. Environ.*, *32*(24), 4245–4264.

Tost, H., M. G. Lawrence, C. Brühl, P. Jöckel, the GABRIEL Team, and the SCOUT-O3-DARWIN ACTIVE Team (2010), Uncertainties in atmospheric chemistry modelling due to convection parameterisations and subsequent scavenging, *Atmos. Chem. Phys.*, *10*, 1931–1951.

Waldteufel, P., and H. Corbin (1979), On the analysis of single-Doppler radar data, *J. Appl. Meteorol.*, *18*, 532–542, doi:10.1175/1520-0450(1979)018<0532:OTAOSD>2.0.CO;2.

Wernli, H., and H. C. Davies (1997), A Lagrangian-based analysis of extratropical cyclones. I: The method and some applications, *Q. J. R. Meteorol. Soc.*, *123*, 467–489, doi:10.1002/qj.49712353811.

Wert, B. P., A. Fried, S. Rauenbuehler, J. Walega, and B. Henry (2003), Design and performance of a tunable diode laser absorption spectrometer for airborne formaldehyde measurements, *J. Geophys. Res.*, *108*(D12), 4350, doi:10.1029/2002JD002872.

Wisthaler, A., et al. (2008), Technical Note: Intercomparison of formaldehyde measurements at the atmosphere simulation chamber SAPHIR, *Atmos. Chem. Phys. 8*, 2189–2200, doi:10.5194/acp-8-2189-2008.